Journal for ImmunoTherapy of Cancer

Dysregulated expression of the tumor suppressor p14ARF in cancer provides an effective target for TCR-T cell therapeutics

Thomas M Schmitt ,[1] Kelsey Furiya,[1] Cheryl Black,[1] Angie Vazquez,[1] Jaishree Sharma,[1] Menna Hailemariam,[1] Daniel H Paushter,[1] Lam Trieu,[1] Jennifer Lam,[1] Bo Lee,[1] Kavya Rakhra,[2] Kerry A Whalen ,[2] Naveen K Mehta,[2] Karsten Sauer,[2] Patrick A Baeuerle,[2] Jennifer S Michaelson,[2] Philip D Greenberg,[1,3] Aude G Chapuis [4,5]

To cite: Schmitt TM, Furiya K, Black C, *et al*. Dysregulated expression of the tumor suppressor p14ARF in cancer provides an effective target for TCR-T cell therapeutics. *Journal for ImmunoTherapy of Cancer* 2026;**14**:e013520. doi:10.1136/jitc-2025-013520

► Additional supplemental material is published online only. To view, please visit the journal online (https://doi.org/10.1136/jitc-2025-013520).

PDG and AGC contributed equally.

Accepted 21 January 2026

For numbered affiliations see end of article.

Correspondence to
Dr Thomas M Schmitt;
tschmitt@fredhutch.org

ABSTRACT

Background The CDKN2A gene encodes two canonical tumor suppressors, p16INK4A and p14ARF, which safeguard cells from malignant transformation by inducing cell cycle arrest and apoptosis in response to aberrant growth signals. Paradoxically, many cancers overexpress these proteins when downstream effectors that enforce negative feedback regulation are lost or inactivated. For example, p14ARF, which regulates p53 activation, is aberrantly expressed in more than 50% of tumors with inactivating p53 mutations. Here, we evaluated the feasibility of targeting dysregulated p16INK4A and p14ARF expression using TCR-T cell therapeutics.

Methods We analyzed a panel of p16INK4A- and p14ARF-derived peptides for HLA-A*02:01-associated presentation and recognition by $CD8^+$ T cells. Antigen-specific T cell receptors were isolated from healthy donor repertoires and expressed in primary T cells to assess specificity, functional avidity, tumor recognition, and safety using in vitro T cell functional assays, in vivo tumor models, and an in vivo safety model.

Results We identified a unique and well-presented p14ARF epitope that was consistently detected in the HLA-A*02:01-associated immunopeptidome of cancer biopsies but not in normal tissues. High-avidity ARF-specific TCRs were isolated from the peripheral repertoire of healthy donors, and TCR-transduced T cells mediated potent tumor cell killing in vitro and in vivo in preclinical models. Furthermore, targeting p14ARF-expressing cells did not result in detectable on-target toxicity in an in vivo safety model.

Conclusions These findings demonstrate the feasibility of targeting dysregulated tumor suppressor proteins with TCR-T cell therapeutics and identify p14ARF as a promising target for future therapies.

WHAT IS ALREADY KNOWN ON THIS TOPIC

⇒ TCR-engineered T cell therapies have shown encouraging clinical activity, but identifying tumor-selective antigens that can be safely and effectively targeted remains a central challenge. Tumor suppressor proteins are often aberrantly expressed in cancer following disruption of negative feedback regulation, as exemplified by p53-dependent control of p14ARF and Rb-dependent control of p16INK4A; however, they have been largely overlooked as targets for TCR-based immunotherapy.

WHAT THIS STUDY ADDS

⇒ This study identifies an HLA-A*02:01-restricted p14ARF-derived epitope that is efficiently processed and presented by tumor cells and recognized by TCR-T cells. ARF_{35-43}-specific TCR-T cells mediate potent, antigen-dependent tumor cell killing in vitro and in vivo with a low risk of off-target reactivity.

HOW THIS STUDY MIGHT AFFECT RESEARCH, PRACTICE OR POLICY

⇒ These findings identify p14ARF as a promising target for immunotherapeutic development, especially for cancers driven by inactivating p53 mutations and human papillomavirus (HPV)-associated tumors. More broadly, this work establishes dysregulated tumor suppressors as a clinically relevant class of targets for TCR-based cell therapies.

INTRODUCTION

TCR-engineered T cells offer a powerful approach to treating solid tumors. However, the scarcity of high-quality, cancer-selective target antigens remains a major obstacle to the success of this therapeutic strategy. Optimal targets for TCR-transduced T cell (TCR-T cell) therapy are abundantly and consistently expressed by tumors, absent or only minimally expressed in normal tissues, and contain T cell epitopes that are efficiently presented by common HLA alleles.[1] Many promising targets, including oncogenes like mutant KRAS,[2] play a functional role in promoting tumor growth and survival. By contrast, tumor

suppressor proteins orchestrate the protective cellular responses to oncogenic transformation, and their loss or inactivation is well known to promote tumor initiation and progression.[3] Paradoxically, tumor suppressors can also be aberrantly overexpressed in many cancers, often when downstream effectors are inactivated and can no longer enforce negative feedback regulation.[4 5] However, tumor suppressors remain an under-explored potential source of tumor-associated antigens.

The *CDKN2A* gene encodes two potent tumor suppressors: p16INK4A (p16) and "Alternate Reading Frame" protein p14ARF (ARF). The CDKN2A locus is unusual in that each of these gene products has its own promoter and unique exon 1, which is spliced to the same exons 2 and 3 but in different reading frames, resulting in no sequence homology at the protein level. Oncogene activation can drive high-level expression of both proteins, both of which play essential non-redundant roles in protecting cells from malignant transformation. p16 arrests cell division through association with cyclin-dependent kinase 4 and 6 (CDK4/6), which blocks retinoblastoma protein (Rb) phosphorylation and cell cycle progression; while ARF activates p53-dependent pathways by inhibiting MDM2-mediated p53 degradation, thereby stabilizing and activating p53.[6] Despite these critical tumor-suppressive functions, one or both proteins are overexpressed in a surprisingly high proportion of cancers.[7–9] For example, in human papillomavirus (HPV)-induced tumors, Rb inactivation by HPV E7 disrupts a negative feedback loop that normally limits E2F-driven p16 expression, resulting in constitutively high levels of p16 protein in HPV-transformed cells.[10] Likewise, oncogene-driven ARF expression results in p53 stabilization/activation, which then normally acts to extinguish ARF expression. Inactivation of p53 disrupts this negative feedback mechanism, resulting in unconstrained ARF overexpression. As a result, ARF is overexpressed by many tumors, including essentially all HPV-positive cervical cancers,[11] more than two-thirds of breast cancers,[12] and the majority of all cancers with inactivating mutations in p53,[5 13] which is the most commonly mutated gene in cancer and found in ~50% of all malignancies.[14] While both p16 and ARF are highly expressed in a broad spectrum of tumors, these proteins have very limited expression in healthy adult tissues.[15 16] Consequently, both proteins could potentially serve as tumor-associated antigens for T cell receptor (TCR)-based immunotherapies, enabling selective targeting of the many tumors harboring inactivating mutations in these canonical tumor suppressor pathways.

To develop TCR-based therapeutics targeting p16 or ARF, we set out to identify and characterize CD8 T cell epitopes from p16 and ARF presented by HLA-A*02:01:01 (HLA-A2). These efforts identified $ARF_{35\text{-}43}$, an ARF-restricted epitope that is efficiently presented by a broad spectrum of HLA-A2^{+} tumor cells. $ARF_{35\text{-}43}$-specific TCR-T cells effectively eliminated ARF-expressing tumors in vitro and in vivo, and T cell-mediated targeting of ARF-expressing cells in vivo proved to be safe in a murine safety model. These findings validate ARF as a novel therapeutic target and highlight the broad potential of overexpressed dysregulated tumor suppressors as a novel class of targets for TCR-T cell-based therapeutics.

METHODS

Mice

All tumor xenograft NSG mouse experiments were completed using NOD.Cg-Prkdc^{scid} Il2rg^{tm1Wjl}/ScJ (NSG) strain mice (The Jackson Laboratory, cat# 005557).

Female Jedi mice (STOCK Ptprc^{a} Tcrb^{Ln1Bdb} Tcra^{Ln1Bdb} H2^{d}/J) strain #028062 and Female B10.D2 mice (B10.D2-Hc^{0} H2^{d} H2-T18^{c}/oSnJ) strain #000461 were used at 6–10 weeks of age. ARF-GFP$^{+/-}$ mice were from established colonies. Since Jedi T cells recognize $_{GFP200\text{-}20}$6 presented on H-2K^{d}, all ARF-GFP$^{+/-}$ mouse experiments were done in F1 progeny B10.D2 background as originally reported.[17]

Antibodies and reagents

Peptides for p16 and ARF described epitopes were obtained from Elim Biopharmaceuticals and HLA-A2/peptide tetramers were produced in the Immune Monitoring Lab at the Fred Hutchinson Cancer Center. The Fred Hutchinson Immune Monitoring Core also prepared $GFP_{200\text{-}206}$/H-2K^{d} tetramer conjugated to PE. All compensation was performed with UltraComp eBeads (eBioscience, cat# 01-2222). Samples were acquired with a BD FACSymphony A3, BD FACSymphony S6, or Canto II using BD FACSDiva software.

Generation of antigen-specific T cell lines

Human PBMCs were purchased from STEMCELL Technologies. These cells are provided as ethically sourced primary human cells collected from consented donors under protocols approved by appropriate ethics review boards, with written informed consent obtained in accordance with the Declaration of Helsinki. Samples were supplied in a deidentified format, and no donor-identifiable information was accessible to the investigators. Mature DCs (DCs) were first generated in vitro by culturing monocytes in DC media (AIM-V media supplemented with 1% human serum) along with the cytokines TNFα, IL-1β, IL-6, and PGE2. The DCs were harvested after 2 days and loaded with 2.5 µg /mL of peptide for 4 hours. The antigen-specific T cell lines were generated by stimulating donor-derived CD8^{+} T cells with the peptide-pulsed DCs. The T cell lines were expanded by feeding the cells with T cell media (RPMI supplemented with 10% human serum) along with IL-2, IL-7, and IL-15 every 2–3 days. After 10–14 days of expansion, the T cell lines were restimulated with irradiated autologous PBMCs pulsed with the relevant peptide. Three rounds of restimulation and expansion were performed before sorting antigen-specific cells. The presence of p16 or ARF-specific T-cells was assessed after each round of stimulation by staining with MHC-peptide tetramers and

analyzing by flow cytometry. To evaluate the immunogenicity and antigen processing/HLA-A2 presentation of candidate epitopes derived from p16 and ARF, we generated polyclonal CD8$^+$ T cell lines specific for each peptide. Four HLA-A*02:01$^+$ healthy donors were used to generate T cell lines in separate experiments. For each antigen, T cell lines showing the highest tetramer mean fluorescence intensity were sorted and used for functional assays. Selected lines for each epitope did not necessarily derive from the same donor.

T cell repertoire analysis and single-cell RNAseq

High-affinity TCR clonotypes were identified from antigen-specific T cell lines that had been sorted using titrated concentrations of tetramer and, in some cases, CD8-independent tetramer made with an HLA-A2 protein containing D227K/T228A mutations in the α3 domain of A2.[18] TCR repertoire analysis was performed on sorted cells using Adaptive Biotechnologies ImmunoSeq platform (to maximize the number of cells/genomes counted for each (clonotype)[19] and 10x genomics immune profiling to identify and quantitate sorted TCRβ clonotypes including paired *TRA/TRB* gene sequence information. Clonotypes that were highly enriched in tetramer sorted populations or increasingly enriched in populations stained with limiting concentrations of tetramer or CD8-independent tetramer were selected for gene synthesis and functional analysis. 10x genomics single-cell RNAseq was performed to identify paired *TRA/TRB* gene sequences for synthesis by the Fred Hutchinson Cancer Center Genomics & Bioinformatics Core using the Chromium Single Cell Human TCR Amplification Kit (10x Genomics, cat# 1000252).

Lentivirus production and transduction

The lentivirus was packaged using 293T cells (ATCC, CRL3216), which were plated (2.2×10^6 cells) in 293T media (RPMI supplemented with 5% FBS and 5% human serum) on 10 cm culture plates and allowed to adhere overnight. The cells were then transfected with sequence-verified DNA plasmids using the Effectene Transfection Reagent (Qiagen, cat#301425). 24 hours post-transfection, the media was replaced with T cell media (RPMI supplemented with 10% Human serum). The following day, virus-containing supernatants were collected and filtered through a 0.45 µm-pore-size Nalgene Syringe filter (ThermoFisher Scientific, cat# 723-2545). Lentiviral transduction of T-cells was performed in 12-well plates with addition of IL-2 (50 IU/mL Aldesleukin, UW Pharmacy) and polybrene (5 µg/mL, Milliporesigma, cat# TR1003G). To facilitate lentiviral transduction, T cells were centrifuged with the virus-containing supernatant for 90 min at 1000 g at 30°C.

GFP-expressing lentivirus was made by the Fred Hutchinson Vector Core.

T cell functional assays

Calculation of functional avidity by Peptide dose-response: Functional avidity was assessed using TCR-transduced CD8$^+$ T-cells or T-cell-derived reporter line Jurkat-Nur77t (CD8-transduced Jurkats lacking endogenous TRA and TRB genes and expressing GFP under the control of the endogenous Nur77 locus). After overnight stimulation with titrated concentrations of peptide, T cell activation was measured by flow cytometry using CD137 expression and GFP levels, respectively. For Jurkat-Nur77t stimulation, the A2$^+$ LCL cell line T2 was added as an APC at a 1:1 ratio. The resulting values were plotted, analyzed, and EC50 values were calculated for each TCR by nonlinear regression analysis using GraphPad Prism Software.

Tumor cell/T cell coculture and Intracellular cytokine staining: Tumor recognition by TCR-T cells was evaluated by intracellular IFNγ staining by flow cytometry. TCR-transduced T cells were cultured with target tumor lines at a 1:1 ratio for 4 hours in the presence of Golgi Plug (Fisher Scientific, cat# BDB555029) and Golgi Stop (Fisher Scientific, cat# BDB554724). Cells were then stained with anti-CD8 antibody, fixed, and permeabilized using the BD Cytofix/Cytoperm fixation/permeabilization solution kit (Fisher Scientific, cat#BDB554714); followed by intracellular staining with an anti-IFNγ antibody (BioLegend, Pacblue anti-human IFNγ clone 4S-B3, cat# 502522). Samples were analyzed by flow cytometry.

Incucyte assay: Target tumor lines were lentivirally transduced with NucGreen fluorescent stain (Sartorius Corporation, Incucyte Nuclight G lenti-puro, cat# 4475) and purified fluorescent cell lines were seeded in a 48-well plate at a density of 10 000 cells per well. TCR-transduced T cells were then added at various E:T ratios as indicated, with each condition plated in triplicate. Total green fluorescence area was measured over the course of a week using the Incucyte system (Sartorius Corporation). The total green area was measured and plotted to assess tumor elimination over time using GraphPad Prism Software.

T cell specificity/cross-reactivity studies

X-scan analysis: An x-scan assay was performed to identify potential cross-reactivity by sequentially replacing each amino acid in the ARF peptide sequence with each of the 19 other amino acids. Peptides were synthesized (Pepscan), and CD8$^+$ TCR-transduced T-cells were stimulated overnight with each peptide at 1 µg/mL. T cell activation was assessed by measuring surface expression of CD137 (BioLegend, PE/Cyanine7 anti-human CD137 clone 4B-1, cat# 309818) by flow cytometry. Amino acid changes at each position that resulted in at least 20% of the T cell response to wild-type peptide were included in a search string entered into the ExPASy ScanProsite tool (http://prosite.expasy.org/scanprosite/) to search the human proteome for potentially cross-reactive peptides.

Alloreactivity screen: The TCRs of interest were co-cultured for 12–16 hours in a 1:1 ratio of CD8+T cells with an extensive panel of B-LCLs (obtained from the Fred Hutchinson Research Cell Bank) expressing different HLA types. After incubation, cells were stained with tetramer, CD8 (BioLegend, Brilliant Violet 421 anti-human CD8α clone RPA-T8, cat# 301036), and CD137

antibodies and analyzed via flow cytometry to test for alloreactivity against non-HLA-A2 alleles.

In vivo functional studies in NSG mice

Female NSG mice aged 6–8 weeks were intraperitoneally (IP) injected with sort-purified GFP-luciferase+/HLA-A2^{+} ARF-expressing tumor cell lines 10–21 days before T cell injection. Tumor growth was monitored weekly by injecting mice with luciferin (150 mg/kg) and visualizing tumor fluorescence using an IVIS Spectrum imaging System (Perkin Elmer) until termination with euthanasia. On day 0, the experimental mice were injected IP with sort-purified TCR-expressing T cells (CD8 only, or 1:1 CD8:CD4 T cells) expanded in 6-well G-Rex plates (Wilson Wolf, cat# 80240M). 6 days post-T cell injection, the mice were bled retro-orbitally and the blood processed, stained with antibodies, and analyzed via flow cytometry. At least 14 days after the first T cell injection, the mice received a second IP injection of sort-purified TCR-expressing T cells, and blood was again collected and analyzed 6 days postinjection. Weekly IVIS imaging continued until the mice met euthanasia requirements. On euthanasia, the remaining tumors were collected in 10% formalin solution-neutral buffer (Sigma-Aldrich, cat# HT501128) for IHC staining.

Jedi/ARF-GFP mouse studies

Mouse splenic T cells isolated from Jedi/B10.D2 mice were stimulated with anti-CD3 (BD Pharmingen, cat# 553058) and anti-CD28 antibodies (BD Pharmingen, cat# 553295) for 7 days in the presence of IL-2 prior to injection; or Naïve Jedi or B10.D2 CD8^{+} T cells were injected along with 1×10^{8} infectious units (IU) of GFP-expressing lentivirus to prime and expand JEDI T cells in vivo. T cells were checked for antigen recognition by measuring intracellular cytokine stimulation in response to titrated peptide. T cells from either Jedi or B10.B2 mice were injected into Arf-GFP$^{+/-}$ mice as indicated, and mice were weighed daily. Mouse blood was collected for glucose monitoring every 3 days, and as indicated for CBCs. Serum samples were submitted to Moichor (San Francisco, CA) for a comprehensive metabolic panel (Moichor Animal Diagnostics service).

Immunohistochemistry

Mouse tissues were fixed in 10% formalin solution-neutral solution (Sigma-Aldrich, cat # HT501128) for at least 48 hours and transferred to 70% ethanol. All tissues were embedded, processed, and stained for IHC by the Experimental Histology Core at Fred Hutchinson Cancer Center.

Mouse tissue collection and lysis

Testes were collected from one pair of approximately 9-month-old, male WT and Arf-GFP$^{+/-}$ mice following standard procedures, then snap-frozen and stored in the vapor phase of liquid nitrogen. Tissues were thawed, weighed, and lysed at a 1:10 mass:volume ratio in a cold solution of Pierce IP Lysis Buffer (Thermo Scientific, 87787) supplemented with cOmplete Mini EDTA-free Protease Inhibitor Cocktail (Roche, 11836170001) and Phosphatase Inhibitor Cocktail II (Abcam, AB201113-1ML) using approximately 30 revolutions of a 1 mL PYREX Glass Pestle Tissue Grinder (Corning, 7724-1) on ice.

Immunoprecipitation/western blot

Pierce Protein G Agarose (Thermo Scientific, PI20398) and ChromoTek GFP-Trap Agarose (Proteintech, gtma-10) were equilibrated following the manufacturers' recommendations and resuspended in complete IP Lysis Buffer. 50 µL of equilibrated Protein G Agarose slurry was added to 300 µL of tissue lysate containing 2.1 mg of total protein. Samples were rotated at 4°C for 2 hours then centrifuged at 2500 rcf and 4°C for 5 min. Precleared lysates were transferred to cold 1.5 mL tubes containing 40 µL of equilibrated GFP-Trap Agarose slurry, while Protein G Agarose was discarded. Samples were rotated for 3 hours at 4°C, then centrifuged at 2500 rcf and 4°C for 5 min. Beads were washed a total of three times with 1 mL of complete IP Lysis Buffer followed by the aspiration of remaining supernatant. Samples were eluted by the addition of 20 µL of LDS Sample Buffer and 20 µL of Dulbecco's Phosphate Buffered Saline (Gibco, 14190-144) and stored at 80°C.

For Western blot analysis, input and IP samples were thawed, and 50% of each was reduced by the addition of Bolt Sample Reducing Agent (10X) (Invitrogen, B0009) and heating at 95°C for 4 min before being cooled on ice. Samples and Precision Plus Protein All Blue Prestained Protein Standards (Bio-Rad, 1610373) were equilibrated to room temperature then loaded on a Bolt 4%–12% Bis-Tris Plus Gel (Invitrogen, NW04120BOX) in a Mini Gel Tank (Invitrogen, A25977). Running was performed at 200 V for 35 min followed by transfer to a Novex Invitrolon 0.45 µm PVDF Membrane (Invitrogen, LC2005) using a Mini Blot Module (Invitrogen, B1000). The membrane was washed three times with ultrapure H2O, shaking for 5 min each time at room temperature, then covered with 10 mL of EveryBlot Blocking Buffer (Bio-Rad, 12010020) and shaken at room temperature for 5 min. Mouse anti-GFP (Roche, 11814460001) and rabbit anti-GAPDH (Proteintech, 10494-1-AP) were diluted 1:1000 and 1:10,000, respectively, in 5 mL of EveryBlot Blocking Buffer and then added to the membrane, which was shaken at 4°C overnight. Following primary antibody staining, the membrane was washed three times, shaking, at room temperature with tris-buffered saline with 0.1% Tween-20 (TBST) prepared from 10 x Tris Buffered Saline (Bio-Rad, 1706435), TWEEN-20 (Sigma-Aldrich, P1379-25ML), and ultrapure water. IRDye 800CW Donkey anti-Mouse IgG Secondary Antibody (LI-COR, 926-32212) and IRDye 680RD Donkey anti-Rabbit IgG Secondary Antibody (LI-COR, 926-68073) were each diluted 1:15 000 in 5 mL of EveryBlot Blocking Buffer containing 0.02% SDS (w/v) (Bio-Rad, 1610418) and 0.2% (w/v) TWEEN-20. A secondary antibody solution was added to the membrane, which was shaken for 1.5 hours at room temperature

in the dark. The membrane was washed 3x with TBST, shaking for 5 min each time at room temperature, and then scanned using an Odyssey CLx Imaging Workstation (LI-COR, 9140-09).

Purification of HLA peptide complexes

Twenty HLA-A*02:01 positive cervical tumor samples that were flash frozen at the time of surgical resection were purchased from DxBiosamples (California, USA). Each tissue was processed as previously described.[20 21] Tissues were pulverized under cryogenic conditions using a mixer mill MM400 (Retch, Germany) and cells were lysed using a detergent buffer (50 mM TRIS pH 8.0, 0.5% IGPAL, 150 mM NaCl, complete protease inhibitor cocktail (Roche, Germany)) for 1 hour at 4°C on a rotary shaker. Lysates were clarified with ultracentrifugation at 200 000 x g for 90 min and a 0.45 µm filtration. Clarified lysates were passed over a W6/32 antibody affinity column and washed extensively with four solvent washes as described in PMID: 31092913. Finally, HLA class I complexes were eluted from the affinity column with 0.2N acetic acid and denatured with heat at 76°C for 10 min. Denatured complexes were loaded on a RP-HPLC system (Shimadzu, Japan) with a 150×2 mm C18 Gemini column (Phenomonex, USA). Peptides were separated and fractionated using a dual linear gradient of Solvent A (2% acetonitrile, 98% water 0.1% trifluoroacetic acid) and Solvent B (95% acetonitrile, 5% water 0.1% trifluoroacetic acid) at a flow rate of 160 µL/min. The gradient consists of 5% Solvent B to 40% Solvent B in 15 min followed by 40% Solvent B to 80% Solvent B in 3 min.

HLA peptide quantification using multiple reaction monitoring LCMS

Seven HLA peptide ligand-containing fractions (fractions 10–16) were dried and resuspended in 10% acetic acid containing 50 fmol/µL heavy isotopically labeled peptides. Heavy and light peptides were purchased from Thermo (Germany) as AQUA peptides. Two heavy labeled peptides in the mixture: 1. An HLA-A*02:01 positive control peptide derived from COPG1 (AIVDKVPSV) and 2. The hARF HLA-A*02:01 peptide (AAPGAPAAV). Labeled amino acids are shown in bold. Once resuspended, 5 µL of sample was injected for nano-scale LCMS using an Eksigent 425 nano HPLC with a trap and elute method in line with a Sciex 6500+QQQ mass spectrometer. Trap columns were EXP2 NANO C18, 2.7 µm (Optimized Technologies, USA) and the analytical column was an Acuity UPLC M-class 75×150 mm HSS T3 C18 1.8 µm (Waters, USA). Samples were eluted with a dual linear gradient of Solvent A (100% water 0.1% formic acid, 5% DMSO) and Solvent B (95% acetonitrile, 5% water, 0.1% formic acid, 5% DMSO). The gradient was 2%–40% Solvent B in 40 min and 40%–80% Solvent B in 2 min. Eluate was ionized using electrospray ionization with an Optiflow (Sciex, Canada) ion source. The 6500 was operating in multiple reaction monitoring (MRM) mode using transitions previously determined from fragment spectra (online supplemental figure 10) with a total cycle time of 1.05 s. All data were interpreted using Skyline-daily. Peak areas for the heavy and light peptides were determined for all samples, and using the light-to-heavy ratio, the molarity of the peptides was determined from the ratio using a 20-point standard curve. The number of HLA peptide complexes was estimated from the moles of peptide assuming a 25% loss of complexes during the purification process and that 1 g of tissue is equal to 5×10^7 cells. Tumor samples in this study were analyzed using targeted MRM to maximize sensitivity for the ARF peptide, while normal tissues were evaluated using a large data-independent aquisition (DIA)-based LC–MS/MS immunopeptidomics dataset (>300 samples) generated with approximately three-fold higher peptide input to partially compensate for the lower per-peptide sensitivity of DIA relative to MRM. The extensive sampling of normal tissues provides high confidence that peptides present in normal tissues would have been detected.

RESULTS

Evaluation of peptides from p16 and ARF proteins predicted to bind HLA-A2

To identify peptides from p16 and ARF that can be presented by HLA-A2, we evaluated a set of 12 p16 peptides and four ARF peptides predicted to bind HLA-A2 using NetMHCpan4.1[22] (figure 1a, online supplemental figure 1), including several overlapping peptides from positions 50-65 of p16, a region previously targeted by a peptide vaccine shown to elicit $CD8^+$ T cell responses in some patients.[23] For each peptide, healthy $CD8^+$ T cells from HLA-A*0201$^+$ donors were stimulated with peptide-pulsed autologous dendritic cells (DCs) and further enriched and expanded with 2–3 additional rounds of peptide restimulation as described previously[24] and tetramer-based cell sorting followed by expansion with our commonly employed T cell rapid expansion protocol.[25] All selected peptides proved capable of binding HLA-A2 and expanding an antigen-specific T cell population from peripheral blood mononuclear cells (PBMCs) that could bind p16 or ARF (p16/ARF) peptide/HLA-A2 tetramers (figure 1b,c). These tetramer$^+$ T cell lines were used to determine whether the selected peptides are naturally processed by the proteasome of target cells and presented by HLA-A2. To assess p16 epitope processing/presentation, tetramer positive T cells were cultured with MDA-MB-231 cells, which have a homozygous deletion of the CDKN2A locus, or MDA-MB-231 cells transduced to express doxycycline-inducible p16 (online supplemental figure 1a). To assess ARF epitope presentation, T cells were cultured with HLA-A2-transduced HeLa cells (HeLa-A2), or HeLa-A2 cells knocked out for ARF expression (online supplemental figure 2a and b). Tetramer$^+$ T cell lines were also cultured with peptide-pulsed target cells to define maximal reactivity. For each epitope, antigen-specific T cell lines were assessed for both activation-induced IFNγ production and activation-induced TCR

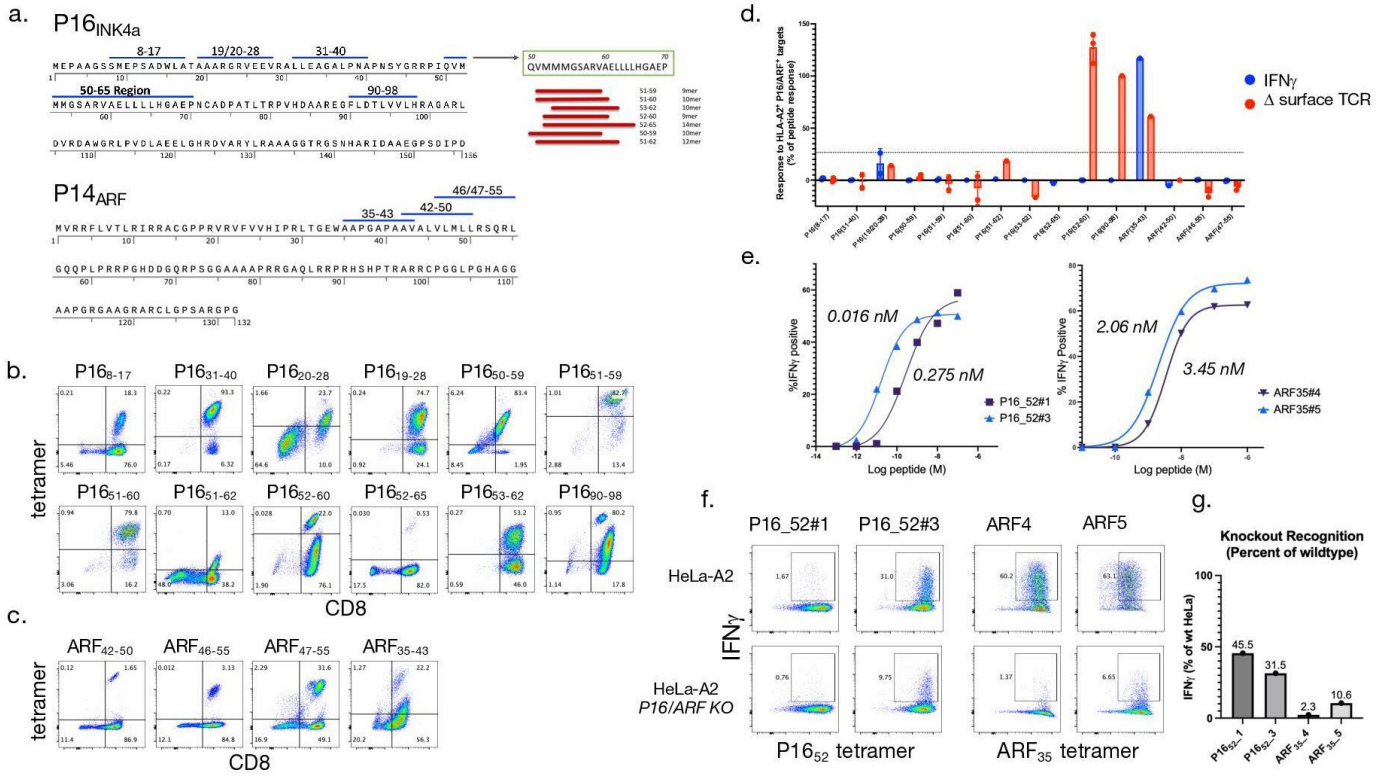

Figure 1 Recognition of predicted HLA-A2-binding peptides by T cells (a) Overview of predicted HLA-A2-binding peptides within the p16 and ARF protein sequences, including several overlapping peptides within the $p16_{50-65}$ region. (b) Peptide/HLA-A2 tetramer binding of polyclonal T cell lines specific for p16 peptides generated by in vitro priming and expansion in response to peptide-pulsed autologous APCs followed by enrichment by flow-cytometric cell sorting. (c) Peptide/HLA-A2 tetramer binding by ARF-specific T cell lines. (d) Recognition of naturally processed and presented p16 and ARF epitopes by T cell lines specific for each. T cell production of IFNγ and down-modulation of surface TCR expression in response to antigen-positive HLA-A2$^+$ target cells compared with antigen-negative HLA-A2$^+$ target cells is shown, presented as a percentage of the maximal response obtained by pulsing target cells with peptide. The dotted line indicates the limit of blank, defined as the 95th percentile of normalized antigen-negative control responses. (e) Functional avidity calculation for primary CD8 T cells transduced to express $p16_{52-60}$- and ARF_{35-43}-specific TCRs. IFNγ production by TCR-transduced T cells in response to titrated concentrations of peptide was measured and fit to a dose-response curve by non-linear regression using Graphpad Prism, from which log peptide EC_{50} was calculated. (f) IFNγ production by TCR-T cells expressing $p16_{52-60}$-specific and ARF_{35-43}-specific TCRs in response to HeLa-A2 cells (top panels) or HeLa-A2 cells made deficient for either p16 or ARF by CRISPR-mediated gene editing (bottom panels). (g) summarizes IFNγ responses from the representative experiment shown in panel (f), normalized to wild-type HeLa cells. No statistical testing was performed, as the data represent a single experiment.

down-modulation from the cell surface (percent tetramer binding), which has been shown to correlate with TCR functional avidity[26] (figure 1d, online supplemental figure 1).

For each epitope, T cell lines responded to peptide-pulsed targets, but most epitope-specific T cells did not recognize p16/ARF-expressing targets in the absence of added peptide. This suggests that these epitopes are generally not efficiently processed and presented by HLA-A2, although in some cases, insufficient TCR affinity could also limit detection. Only T cell lines specific for three p16/ARF peptides recognized antigen-positive target cells without exogenously added peptide: $p16_{52-60}$ and $p16_{90-98}$, which showed strong antigen-specific TCR down-modulation but failed to produce IFNγ in response to either peptide-pulsed or p16-expressing target cells; and ARF_{35-43}, which elicited T cells that both produced IFNγ and down-modulated TCR surface expression in response to ARF-expressing target cells (figure 1d).

p16 is expressed in the thymus, and its expression by senescent cells in normal tissues increases with age,[27] so the failure of $p16_{52-60}$-specific T cells to produce IFNγ following antigen encounter despite TCR down-modulation may reflect a form of central or peripheral T cell tolerance. To formally assess TCR-mediated T cell activation and antigen-specific killing by functional T cells, TCR-encoding genes (*TRA* and *TRB*) from $p16_{52-60}$, $p16_{90-98}$ and ARF_{35-43} tetramer$^+$ clonotypes were isolated for genetic transfer into donor PBMCs. Antigen-specific T cell lines were sorted for T cells binding high levels of each peptide-HLA-A2 tetramer, from which paired TCR gene sequences were identified by single cell RNA sequencing (10x Genomics). Two antigen-specific TCRs each were identified and characterized from both

$p16_{52\text{-}60}$ and $ARF_{35\text{-}43}$-specific lines. One $p16_{90\text{-}98}$-specific TCR was also identified, but it exhibited poor tetramer binding and function and was not pursued further.

Porcine teschovirus-1 2A (P2A)-linked codon-optimized lentiviral expression vectors were constructed and lentivirus was generated for transducing donor $CD8^+$ T cells. For each p16 or ARF-specific TCR-transduced T cell population, functional avidity was assessed by measuring IFNγ production in response to titrated peptide to calculate an EC_{50} value (figure 1e). The calculated EC_{50} values for these TCRs ranged from 0.016 nM to 3.45 nM, which should be sufficient to mediate effective T cell activation in response to a well-presented target.[28] TCR-T cells were co-cultured with HeLa-A2 cells, or HeLa-A2 cells knocked out for expression of p16 or ARF (online supplemental figure 2a and b). TCR-T cells expressing $TCR_{p16\_52\#3}$ but not $TCR_{p16\_52\#1}$ produced IFNγ in response to HeLa-A2 cells (figure 1f), and this response by $TCR_{p16\_52\#3}$ was decreased, but not eliminated, when HeLa-A2 cells deficient for p16 were targeted (figure 1g). This suggests that an alternate antigen was also being recognized.

A search for similar peptides in the human proteome revealed that the related protein CDKN2B (p15) contains a peptide identical to $p16_{52\text{-}60}$, which is also expressed by HeLa cells.[29] $p16_{52\text{-}60}$ is therefore not specific for p16, which may contribute to the lack of effector function observed for $p16_{52\text{-}60}$-specific T cells, and consequently, this epitope is unsuitable as a therapeutic target. In contrast, the $ARF_{35\text{-}43}$ peptide is unique in the human proteome, and both $ARF_{35\text{-}43}$-specific TCRs induced robust IFNγ responses against HeLa-A2 cells (figure 1f). These responses were greatly reduced when targeting HeLa-A2-ARF KO cells, especially for TCR_{ARF4} TCR-T cells, for which the response was reduced by ~98% (figure 1g). Although some potential cross-reactivity (1.37%) was detected for ARF4 in this experiment prompting further safety studies (described in figure 2), these results suggested that the $ARF_{35\text{-}43}$ epitope is well-presented, and that $ARF_{35\text{-}43}$-specific TCR-T cells appear

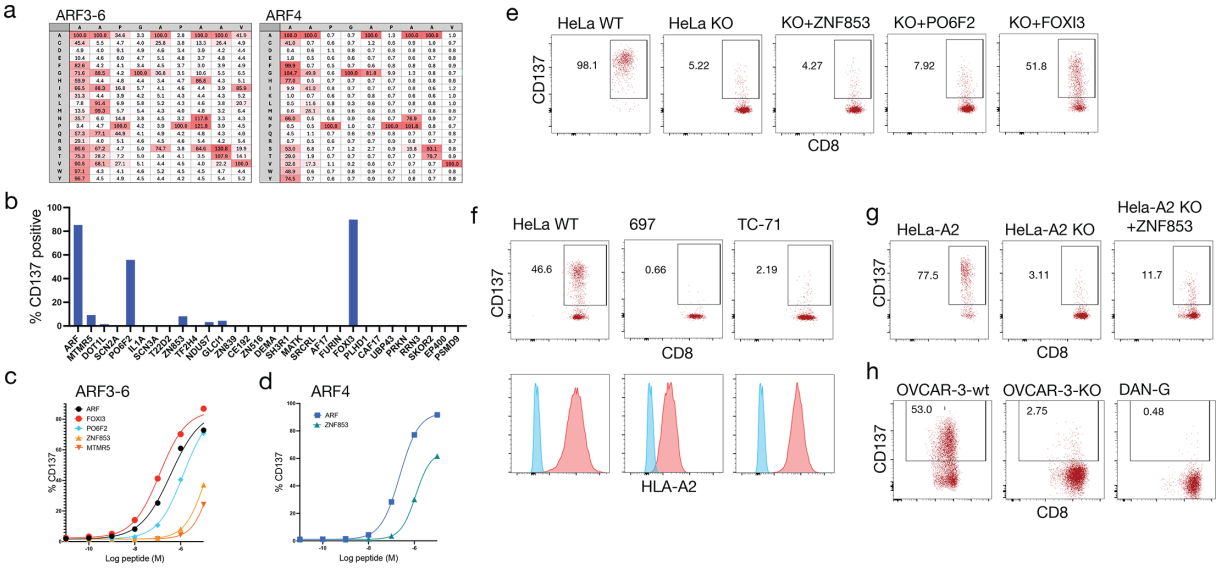

Figure 2 Safety and specificity of $ARF_{35\text{-}43}$-specific TCR-T cells in vitro. (a) Results of x-scan analysis of $TCR_{ARF3\text{-}6}$ and TCR_{ARF4} TCRs. For each position of the $ARF_{35\text{-}43}$ peptide the original residue is listed in the gray bar at the top of each column, and all 20 possible amino acid substitutions are listed in the gray bar to the left. TCR-T cells were cultured overnight with peptides containing the indicated substitution at each position of the ARF peptide, and CD137 expression was determined by flow cytometry and presented as a percentage relative to the T cell response to wild type peptide. This value is indicated in each corresponding box, with red shading corresponding with the relative magnitude of response. Based on these results, the human proteome was screened for all peptides containing permissive residues (resulting in >20% reactivity in the x-scan) at each position, and 30 potential HLA-A2-binding cross-reactive peptides were identified for $TCR_{ARF3\text{-}6}$ (b) The identified peptides were synthesized and tested for the ability to activate $TCR_{ARF3\text{-}6}$ TCR-T cells to produce IFNγ following overnight culture. (c) For peptides that induced IFNγ production by more than 5% of cells, a dose-response assay was performed to determine the relative functional avidity of $TCR_{ARF3\text{-}6}$ for each peptide (d) Only one potential cross-reactive peptide was identified for TCR_{ARF4} (from ZNF853), for which a similar analysis was performed. (e) Activation-induced CD137 expression by TCR-T cells expressing $TCR_{ARF3\text{-}6}$ following coculture with control HeLa-A2 or ARF-deficient HeLa-A2 KO cells alone or lentivirally transduced to express cross-reactive peptide-containing 5' fragments of ZNF853, PO6F2, or FOXI3 genes under a strong murine stem cell virus (MSCV) promoter. (f) Activation-induced CD137 expression by $TCR_{ARF3\text{-}6}$ TCR-T cells following coculture with control A2-HeLa or $HLA\text{-}A2^+$ ARF^- tumor cell lines 697 and TC-71 (top panels), which naturally express relatively high levels of FOXI3 transcripts compared with other tumor cell lines (online supplemental figure 3d). Lower panels show the HLA-A2 surface expression for each cell line (red) compared with an unstained control (blue). (g) Activation-induced CD137 expression by TCR_{ARF4} TCR-T cells following coculture with control HeLa-A2 cells, ARF-deficient HeLa-A2 KO cells, or HeLa-A2 KO cells transduced with ZNF853. (h) Activation-induced CD137 expression by TCR_{ARF4} TCR-T cells following coculture with control OVCAR-3 cells (ARF^+ $ZNF853^+$ $HLA\text{-}A2^+$), OVCAR-3 cells made deficient for ARF, or the $HLA\text{-}A2^+$ ARF^- $ZNF853^+$ tumor cell line DAN-G.

to be both highly potent and ARF-specific. Efficient presentation of this epitope is further demonstrated by studies that useliquid chromatography–mass spectrometry (LC–MS) to identify peptides eluted from tumor-derived surface MHC molecules. Several of these studies list ARF_{35-43} among identified peptides.[30–32] Collectively, these findings indicate that ARF_{35-43} is a unique A2-restricted epitope efficiently presented by ARF-expressing tumors. Thus, this epitope was selected for further evaluation as a therapeutic target.

High affinity ARF_{35-43}-specific TCRs mediate robust in vitro antitumor activity by TCR-T cells

We next generated ARF_{35-43}-specific $CD8^+$ T cell lines from eight additional healthy donors to identify potentially more potent and specific TCR candidates that have both high affinity for ARF_{35-43} and lack off-target recognition or alloreactivity. To identify TCR clonotypes that bind the A2-presented ARF peptide with high affinity, antigen-specific T cell lines were stained with titrated concentrations of ARF_{35-43} peptide/HLA-A2 tetramer or with CD8-independent tetramer and sorted based on tetramer binding. Clonotype frequency within sorted populations was determined by immunoseq (Adaptive Biotech)[19] and *TRA/TRB* gene pairing was determined by 10x single-cell immune cell profiling (10x Genomics). TCR clonotypes selectively enriched within sorted populations that had been stained with limiting tetramer concentrations or CD8-independent tetramer were preferentially selected for synthesis and functional analysis. Seventeen TCRs were synthesized as codon-optimized, TCRβ-p2a-TCRα lentiviral expression constructs. To assess expression and measure functional avidity for each TCR, a *TRA/TRB* gene-deficient, *CD8A/CD8B* transduced Jurkat T cell line was used, which has green fluorescent protein (GFP) knocked into the *NUR77* locus as a reporter for TCR signal strength[33] (referred to hereafter as Jurkat-Nur77t cells). To determine the functional avidity of each TCR, GFP expression by TCR-transduced Jurkat-Nur77t cells was measured following culture with T2 cells pulsed with titrated concentrations of ARF_{35-43} peptide, followed by calculation of comparative EC_{50} values for each TCR (figure 3a).

Nine of the TCRs were responsive to ARF peptide when expressed by Jurkat-Nur77t cells (figure 3a), and four TCRs that had an EC_{50}<100 nM were selected for further functional analysis. To directly compare the antitumor potency conferred by each TCR, primary $CD8^+$ T cells were lentivirally transduced with the four selected TCR constructs. TCR_{ARF4}, which had exhibited high functional avidity and low, potentially background levels of off-target reactivity (figure 1e–g), was also included in this analysis. ARF peptide/A2 $tetramer^+$ TCR-T cells were co-cultured with live GFP-expressing HeLa-A2 or HeLa-A2-ARF KO cells to assess tumor cell killing and ARF_{35-43} specificity (figure 3b,c). TCR_{ARF4}, $TCR_{,ARF2-7}$ and TCR_{ARF3-6} mediated robust elimination of HeLa-A2 cells at both a 1:1 effector-to-target (E:T) ratio (figure 3b, left panel) and at the low E:T ratio of 0.25:1 (figure 3b, right panel). When targeting HeLa-A2-ARF KO cells, TCR-T cell-mediated killing was completely abrogated for TCR_{ARF4} and TCR_{ARF3-6}, despite slightly higher surface expression of A2 on the KO cell line (online supplemental figure 2a). This indicates that HeLa cell killing by these TCR-T cells was ARF specific (figure 3c). On the other hand, TCR_{ARF2-7} exhibited substantial killing of both wild-type HeLa-A2 and HeLa-A2-ARF KO cell lines, suggesting substantial off-target reactivity. TCR_{ARF2-7} was therefore not further evaluated. Next, untransduced control T cells or TCR-T cells expressing TCR_{ARF4} or TCR_{ARF3-6} were cocultured with a panel of $HLA\text{-}A2^+$ tumor cell lines across a diverse range of cancer types with varying amounts of reported CDKN2A expression (figure 3d, online supplemental figure 2b). Expression of the activation marker CD137 was induced on T cells in response to all $CDKN2A^+$ tumor lines except for cervical cancer lines C33a and MS751, which have been reported to have multiple antigen presentation defects,[34] including attenuated A2 gene expression (online supplemental figure 2c). SKMEL5 cells have a homozygous deletion of the CDKN2A locus[35] and served as a negative control. Both TCR_{ARF4} and TCR_{ARF3-6} TCR-T cells efficiently recognized the naturally $HLA\text{-}A2^+$ tumor lines CFPAC-1 and SW480, and TCR-T cell-mediated killing of these tumor lines was assessed in an Incucyte assay (figure 3e f). TCR_{ARF4}- and TCR_{ARF3-6}-TCR-T cells could efficiently kill both tumor cell lines, but SW480 cells were less efficiently targeted by TCR-T cells at the lowest E:T ratio of 1:1 (figure 3f). These results identified TCR_{ARF4} and TCR_{ARF3-6} as therapeutic candidates with high potency and specificity and demonstrated efficient presentation of ARF_{35-43} across multiple tumor lineages, highlighting the potentially broad applicability of TCR-T cell-based therapeutics targeting ARF_{35-43}.

Specificity and safety of ARF_{35-43}-specific TCR-T cells

TCR_{ARF3-6} and TCR_{ARF4} were further evaluated for restricted specificity to the ARF peptide by screening for potential cross-reactivity with other HLA-A2-presented self-peptides. First, an X-scan analysis was performed to identify alternate amino acids that could be substituted within the ARF_{35-43} peptide and would be permissible for recognition by the TCRs.[36] 172 peptides were synthesized in which each position of the ARF_{35-43} peptide was sequentially substituted with every possible alternative amino acid. TCR-T cells expressing TCR_{ARF3-6} or TCR_{ARF4} were cultured with each peptide and CD137 expression was assessed (figure 2a). A degenerate search string was generated by incorporating all residues at each position that resulted in reactivity equivalent to at least 20% of that elicited by wild type ARF, which was then used to probe the human proteome with the ScanProsite tool. For TCR_{ARF3-6}, 60 matching peptides were returned, of which 30 (including ARF_{35-43}) were predicted to efficiently bind to HLA-A2 by NetMHCpan 4.1 (defined as a percentile rank <5) (online supplemental table 2). These 30 peptides were synthesized and tested for recognition

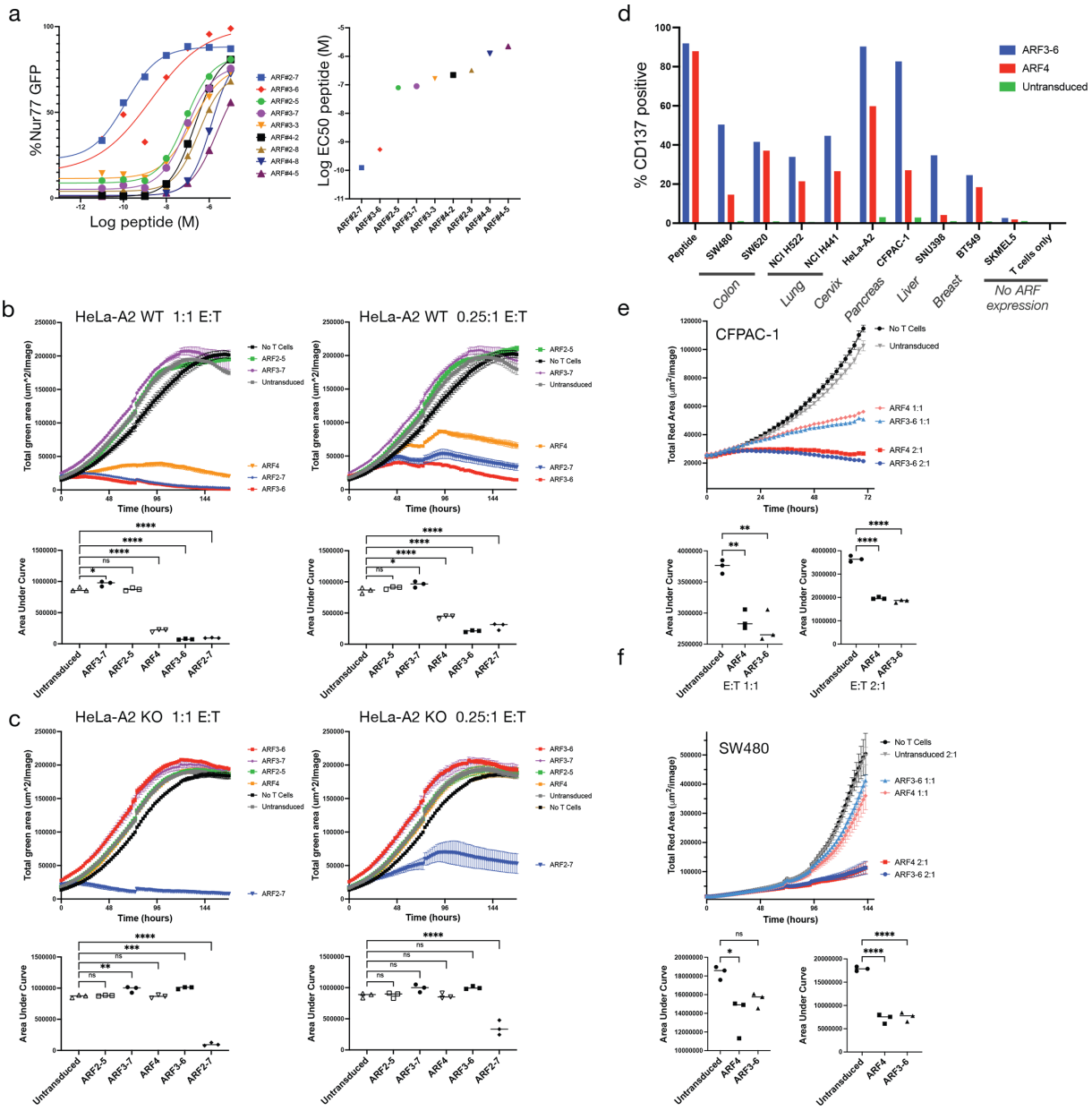

Figure 3 In vitro efficacy of ARF_{35-43}-specific TCR-T cells. (a) $CD8^+$ donor-derived T cells were transduced to express ARF_{35-43}-specific TCRs and functional avidity was then determined by measuring IFNγ production in response to titrated peptide. Curve-fitting of dose-response data and calculation of EC_{50} was performed by non-linear regression using Graphpad Prism. (b) Incucyte assay measuring ARF_{35-43}-specific TCR-T cell killing of GFP-expressing HeLa-A2 cells cocultured for 7 days at an E:T ratio of 1:1 or 0.25:1 as indicated. (c) A similar Incucyte assay measuring ARF_{35-43}-specific TCR-T cell killing of GFP-expressing HeLa-A2 cells deficient for ARF (HeLa-A2-ARF KO cells) (d) CD137 expression by TCR_{ARF3-6} or TCR_{ARF4} TCR-T cells in response to coculture with $HLA\text{-}A2^+$ tumor cells derived from different lineages that naturally express ARF protein, or in that lack ARF expression ($ARF^{-/-}$ cell line SKMEL5 and T cell only conditions). (e,f) Incucyte assay demonstrating TCR_{ARF4} and TCR_{ARF3-6}-mediated T cell lysis of the pancreatic adenocarcinoma cell line CFPAC-1 (e) and the colon adenocarcinoma cell line SW480 (f) at E:T ratios of 1:1 and 2:1 as indicated. For Incucyte assays (b, c, e, and f), total fluorescent area over time is shown, with corresponding area-under-the-curve (AUC) analyses calculated per well over the duration of the assay using a baseline of zero. AUC values were compared using one-way ANOVA with Dunnett's multiple-comparisons test relative to the untransduced T cells as indicated. Statistical significance is denoted as *p<0.05, **p<0.01, ***p<0.001, ****p<0.0001. ANOVA, analysis of variance; E:T, effector-to-target.

by TCR_{ARF3-6} TCR-T cells by measuring activation-induced CD137 expression (figure 2b).

In addition to ARF_{35-43}, four other peptides induced CD137 expression by TCR_{ARF3-6} TCR-T cells above a 5% threshold, and the functional avidity of TCR_{ARF3-6}-T cells for these peptides was determined (figure 2c). Peptides from FOXI3 and PO6F2 were found to be well-recognized by TCR_{ARF3-6}, while MTMR4 and ZNF853 were only recognized at high, non-physiological levels of peptide.[28] For TCR_{ARF4}, only one potential cross-reactive peptide was

identified by ScanProsite, from the protein ZNF853. This peptide was recognized by TCR_{ARF4}, although with lower avidity (~fivefold higher EC_{50}) compared with the ARF_{35-43} peptide (figure 2d). We next tested whether the TCR_{ARF3-6} cross-reactive peptides could be naturally processed and presented on HLA-A2. TCR_{ARF3-6} TCR-T cells were cocultured with HeLa-A2 cells, HeLa-A2-ARF KO cells, or HeLa-A2-ARF KO cells lentivirally transduced to express either the first 453 amino acids of ZNF853, full-length PO6F2, or the first 224 amino acids of FOXI3. Each protein was expressed linked by a P2A element to an open reading frame that included murine Thy1.2, so that Thy1.2 surface expression correlates with expression of each target protein in transduced HeLa-A2-ARF-KO cells (online supplemental figure 3a). ZNF853 and PO6F2 expression by HLA-A2-HeLa cells did not induce TCR_{ARF3-6} TCR-T cell activation, indicating that these peptides are not efficiently processed/presented by HLA-A2 (figure 2e). However, cells transduced to express the FOXI3 fragment did elicit a response from TCR_{ARF36} TCR-T cells, although the response was 50% lower than the response to wild type HeLa-A2 cells (figure 2e, rightmost vs leftmost panels).

In mRNA expression data from the Human Protein Atlas (HPA) (www.proteinatlas.org),[37] FOXI3 is expressed at only low levels by few cell types, including Müller glia cells in the retina and cytotrophoblasts and syncytiotrophoblasts in the placenta (online supplemental figure 3b and c). The highest expression level reported is 10.5 normalized transcripts per million (nTPM) by Müller glia cells, as compared with >500 nTPM of the *CDKN2A* gene detected in many ARF positive tumors.[37] To determine whether TCR_{ARF3-6} TCR-T cells could recognize FOXI3 presented by target cells expressing physiological levels of FOXI3, TCR_{ARF3-6} TCR-T cells were cocultured with the lymphoma cell line 697 and the Ewing sarcoma cell line TC-71, which express 14.1 and 1.6 nTPM of FOXI3, respectively in HPA gene expression data and 10.1 and 2.89 nTPM, respectively in data from the Cancer Dependency Map project (DepMap)[38] (online supplemental figure 3d). These tumor lines express HLA-A2 on the cell surface (figure 2f, lower panels), and FOXI3 protein expression by these cell lines was detectable by western blot (online supplemental figure 3e). These cell lines express FOXI3 at levels similar to the highest expressing normal tissue cell types but did not elicit a TCR-mediated response from TCR_{ARF3-6} TCR-T cells (figure 2f, upper panels). Taken together, these data suggest that TCR_{ARF3-6} TCR-T cells are unlikely to target cells expressing physiological levels of FOXI3. A similar analysis was performed to assess ZNF853 recognition by TCR_{ARF4}. TCR_{ARF4} TCR-T cells recognized HeLa-A2-ARF KO cells that overexpress ZNF853 at low levels (11.7% of TCR-T cells produce low levels of CD137 in response to HeLa-A2-ARF KO+ZNF853 vs 77.5% that expressed high levels of CD137 in response to HeLa-A2) (figure 2g). Furthermore, TCR_{ARF4} TCR-T cells did not recognize DAN-G cells or ARF-deficient OVCAR3 cells (Ovcar3-KO), both of which naturally express high levels of ZNF853 (figure 2h, online supplemental figure 3f). Finally, TCR_{ARF3-6} and TCR_{ARF4} TCR-T cells were tested for alloreactivity against a panel of B-LCL lines derived from donors expressing the most common HLA alleles in the US population (online supplemental figure 3g), and no reactivity was detected against any of the tested cell lines. These data demonstrate that TCR_{ARF3-6} and TCR_{ARF4} are highly specific for ARF_{35-43}, indicating a limited risk of off-target reactivity or alloreactivity for these TCRs.

In vivo tumor regression mediated by ARF_{35-43}-specific TCR-T cells

We have previously shown that a TCR-T cell product consisting of both CD4 and CD8 T cells expressing CD8αβ in addition to transgenic class I-restricted TCR genes can drive a coordinated $CD4^+$ and $CD8^+$ T cell response that results in enhanced in vivo anti-tumor efficacy.[39] To determine the best arrangement of the TCR and CD8 genes in a 2A-linked construct for optimal expression efficiency and functional avidity, lentiviral vectors were constructed expressing P2A-linked *TRA*, *TRB*, *CD8A*, and *CD8B* genes in different positions to determine which resulted in the highest expression/greatest functional avidity (online supplemental figure 4a). A construct with *TCRβ-P2A-TCRα* in the 5' position relative to *CD8A* and *CD8B* exhibited the lowest EC_{50} (online supplemental figure 4b). This construct was selected for further development, and an Incucyte assay was performed to confirm robust tumor killing activity in vitro by TCR-T cells expressing the therapeutic TCR_{ARF3-6}-p-CD8 construct (online supplemental figure 4c). TCR constructs with this design are referred to hereafter as TCR_{ARF4}-p-CD8 and TCR_{ARF3-6}-p-CD8. To assess the in vivo therapeutic activity of ARF-specific TCR-T cell therapy, and to determine the more effective ARF-specific TCR against established tumors in vivo, TCR-T cells expressing TCR_{ARF4}-p-CD8 or TCR_{ARF3-6}-p-CD8 were injected into NSG mice that had been engrafted 3 weeks earlier with luciferase-expressing colon carcinoma-derived SW480 cells, and 2 weeks later a second dose of T cells was injected. Bioluminescence imaging was performed weekly to track tumor burden (figure 4a; online supplemental figure 5a). TCR_{ARF3-6}-p-CD8 TCR-T cells mediated significant attenuation of tumor cell growth with a reduction in tumor burden compared with untransduced T cells, while TCR_{ARF4}-p-CD8 TCR-T cells mediated a more modest reduction (figure 4b), indicating that TCR_{ARF3-6} is the more potent ARF-specific TCR, consistent with the in vitro results (figure 3b,d).

The antitumor efficacy of the more effective TCR_{ARF3-6}-p-CD8 TCR-T cell product was evaluated in a second in vivo model where NSG mice were engrafted with luciferase gene transduced pancreatic cancer-derived CFPAC1 cells. After 10 days, tumor-engrafted mice were injected with sort-purified $CD4^+$ and $CD8^+$ T cells transduced to express either TCR_{ARF3-6}-p-CD8 or an irrelevant TCR P2A-linked with CD8α and CD8β (TCR_{Irr}-p-CD8). Mice were monitored weekly for luciferase activity as a proxy for tumor burden, and after 14 days a second dose of TCR-T cells was given (figure 4c;

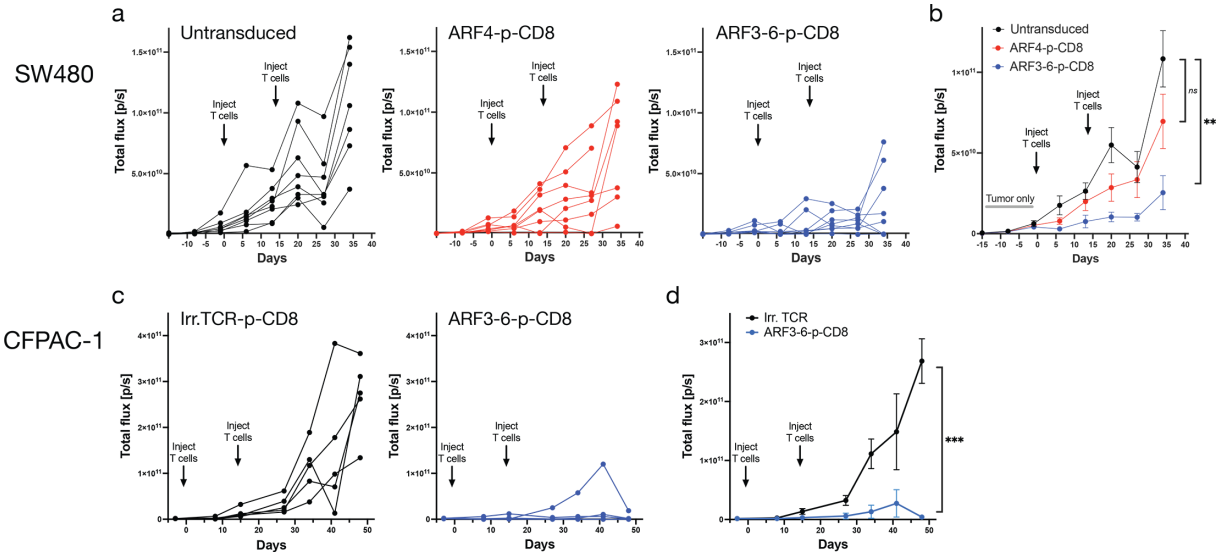

Figure 4 In vivo efficacy of ARF_{35-43}-specific CD4+CD8 TCR-T cells (a) NSG mice were engrafted with 3.0×10^5 SW480-Luc tumor cells, followed 21 days later by treatment with 8×10^6 total cells per mouse of CD4 and CD8 T cells (4×10^6 CD4 T cells and 4×10^6 CD8 T cells) that were untransduced or transduced with either TCR_{ARF4}-p-CD8 or TCR_{ARF3-6}-p-CD8, with eight mice treated per condition. After another 14 days, mice received a second dose of 8×10^6 cells per mouse of CD4 and CD8 T cells (5×10^6 CD4 T cells and 3×10^6 CD8 T cells) (online supplemental figure 5a). Tumor burden was evaluated weekly by bioluminescence imaging as indicated. (b) Total tumor-derived flux (photons/s) for mice treated with untransduced T cells (black), TCR_{ARF4}-p-CD8 (red) or TCR_{ARF36}-p-CD8 (blue) transduced T cells is shown. The mean flux value for each timepoint/condition is shown, with error bars indicating SE of the mean. (c) NSG mice were engrafted with 1.25×10^5 CFPAC-1-Luc tumor cells, followed by treatment with 5×10^6 cells each of CD4 and CD8-T cells that were transduced with either the irrelevant control TCR_{irr}-p-CD8 or with TCR_{ARF3-6}-p-CD8 10 days later. After another 16 days, mice received a second dose of 5×10^6 each of CD4 and CD8 T cells (online supplemental figure 5). Tumor burden was evaluated by bioluminescence imaging on days –3, 8, 15, 27, 34, 41, and 48 as indicated. (d) Total tumor-derived flux (photons/s) for mice treated with TCR_{irr}-p-CD8 TCR-T cells (black), or TCR_{ARF36}-p-CD8 TCR-T cells (blue) is shown. The mean flux value for each timepoint/condition is shown, with error bars indicating SE of the mean. P values were calculated by unpaired t test in GraphPad Prism (ns $p>0.05$; ** $p\leq0.01$; *** $p\leq0.001$).

online supplemental figure 5b). Effective in vivo anti-tumor activity by TCR_{ARF3-6}-p-CD8 but not TCR_{Irr}-p-CD8 TCR-T cells was observed by bioluminescence imaging (figure 4c,d). These data demonstrate that TCR_{ARF3-6} can mediate potent antitumor killing activity both in vitro and in vivo and can therapeutically control ARF^+ tumor growth in two different difficult-to-treat solid tumor models.

Assessing the safety of targeting ARF-expressing cells with T cells in vivo

ARF expression by healthy tissue is very limited. Studies in mice demonstrate that ARF protein is detected during embryonic development of the hyaloid vascular system in the eye with no detection in the eye by postnatal day 7, and in dividing spermatogonia in the testes.[40 41] In adulthood, ARF expression is rare[4 42] but can be associated with senescent cell populations, including some senescent beta cells in pancreatic islets.[43 44] Previous studies have established that elimination of ARF-expressing cells in mice expressing the diphtheria toxin gene knocked into the ARF locus,[43 45] or elimination of p16-expressing cells in mice engineered with inducible suicide genes linked to the p16 locus (INK-ATTAC and p16-3MR),[46–50] does not result in overt toxicity but appears to mitigate several age-related symptoms and extends overall survival. We sought to determine whether treating mice with T cells that can kill ARF-expressing cells is similarly well tolerated. The ARF protein is poorly conserved between mice and humans (~50% homology), and the human ARF_{35-43} epitope is not conserved in mice, precluding the use of TCR_{ARF3-6} in HLA-A2-transgenic mice to directly assess the in vivo safety of TCR_{ARF3-6} TCR-T cells. As an alternative, GFP-specific T cells from 'Just EGFP death-inducing' (JEDI) mice were injected into mice expressing GFP as a gene-specific reporter (ARF-GFP mice).[42] $CD8^+$ JEDI T cells, which are from the $H\text{-}2Kd^+$ B10.D2 strain, express a TCR specific for enhanced GFP $(eGFP)_{200-208}$ presented by H-2Kd and have been used to efficiently eliminate GFP-expressing cells in vivo when injected into the F1 progeny of B10.D2 and C57BL/6 (B6)-derived mice that express GFP as a gene-specific reporter, even when GFP expression is limited to a few cells within distinct tissues including the heart, brain, kidney, pancreas, and liver.[17 51–53]

In ARF-GFP mice (B6 background), exon 1b of ARF is replaced with GFP so that cells expressing ARF are marked by GFP expression. Negligible GFP expression was detected in healthy tissues of these mice other than spermatogonia in adult testes and the hyaloid vasculature in the eyes of newborn mice,[42] consistent with the observation that ARF protein is difficult to detect in most healthy tissues.[41] However, a strong GFP signal was detected in embryonic fibroblasts undergoing senescence after in vitro culture, and tumors that developed in these mice

exhibited vivid green fluorescence, demonstrating the responsiveness of ARF to oncogenic signals in vivo.[42] To confirm ARF promoter-driven GFP expression in heterozygous ARF-GFP mice, testes from ARF-GFP$^{+/-}$ x B10.D2 F1 mice were assessed for GFP protein expression, which was detected in the ARF-GFP$^{+/-}$ but not ARF-GFP$^{-/-}$ testes (online supplemental figure 6a). Mouse embryonic fibroblasts (MEFs) were also generated from ARF-GFP$^{+/-}$ x B10.D2 F1 mid-gestation embryos, and each of three MEF lines from heterozygous ARF-GFP$^{+/-}$ mice contained >40% GFP-expressing cells after 3 weeks of in vitro culture (online supplemental figure 6b), indicating that GFP expression faithfully marks ARF expressing senescent embryonic fibroblasts as previously reported.[42 54]

To evaluate the safety of transferring JEDI T cells into ARF-GFP mice, CD8$^+$ T cells from JEDI or B10.D2 mice were purified and expanded in vitro. GFP-specific functional avidity was first assessed to confirm T cell specificity and function (online supplemental figure 6c), and then T cells were transferred (1×10^{7}T cells/mouse) into the F1 progeny of B10.D2 x ARF-GFP (figure 5a). Engrafted mice were evaluated for 48 days for potential toxicity

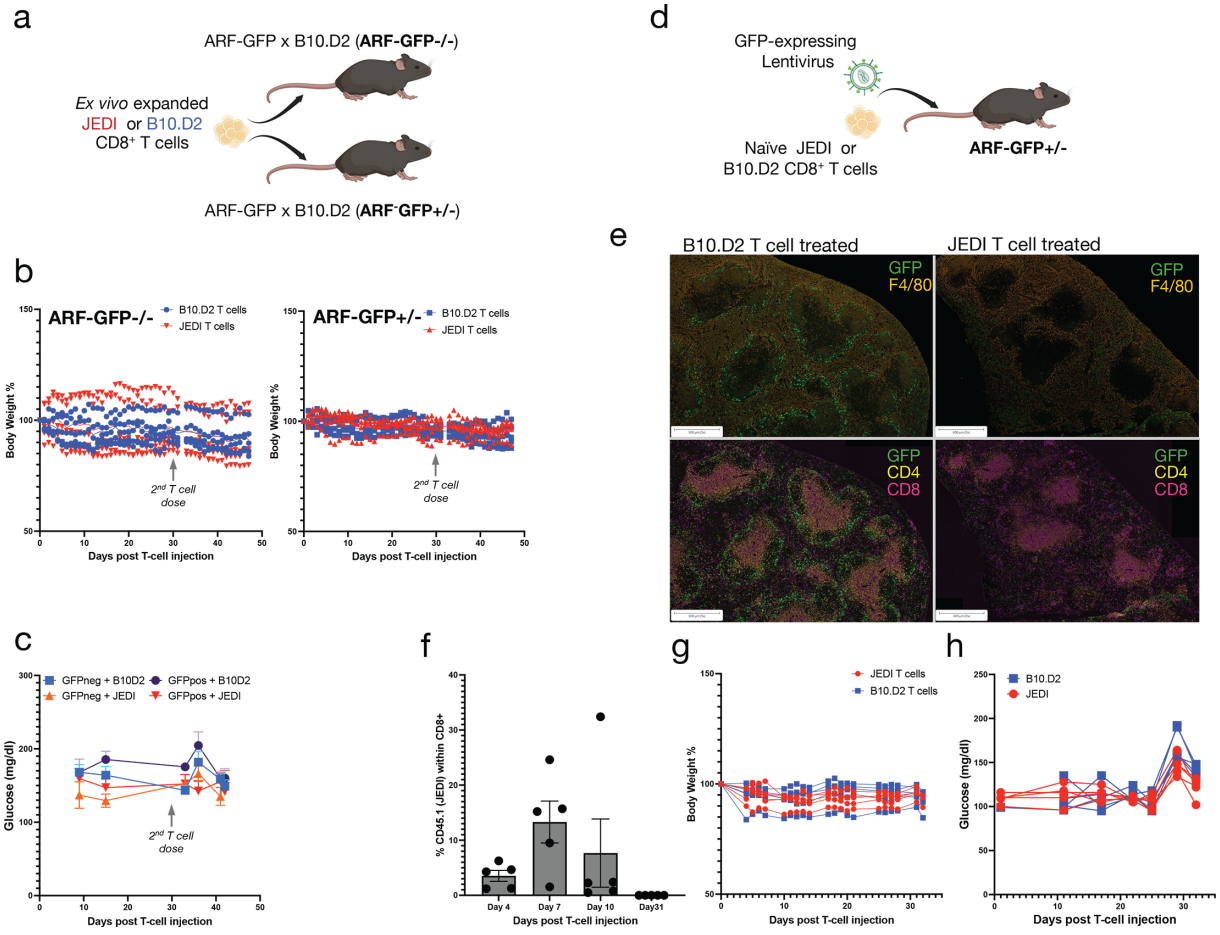

Figure 5 Safety of targeting ARF-expressing cells in vivo. (a) Schematic of T cell transfer experiment with ex vivo expanded JEDI or B10.D2 CD8$^+$ T cells, injected into ARF-GFP$^{+/-}$ or littermate control ARF-GFP$^{-/-}$ mice. Treated mice received a second dose of in vitro-expanded T cells 30 days after the first T cell injection (b) Control ARF-GFP$^{-/-}$ mice (left panel) or ARF-GFP$^{+/-}$ mice (right panel) treated with B10.D2 (blue lines) or JEDI (red lines) T cells were monitored for changes in body weight for 48 days (c) The same groups of mice were monitored for changes in blood glucose at the indicated timepoints. (d) Schematic of T cell transfer experiment with naïve JEDI or B10.D2 CD8$^+$ T cells injected into ARF-GFP$^{+/-}$ mice followed by vaccination with a lentivirus expressing GFP. (e) IHC of spleen sections from ARF-GFP$^+$ mice injected with 10^8 IU of GFP-expressing lentivirus, followed by treatment with control B10.D2 T cells (left panels) or JEDI T cells (right panels) for 32 days. GFP expression is shown in the context of the monocyte/macrophage marker F4/80 staining (top) or with staining for CD4 and CD8 (bottom), as indicated. (f) The percentage of CD45.1$^+$ JEDI T cells detected within the CD8$^+$ subset of blood leukocytes by flow cytometry from JEDI treated ARF-GFP$^{+/-}$ mice at days 4, 7, 10, and 31 after T cell injection as indicated. (g) Mice treated with B10.D2 (blue lines) or JEDI (red lines) T cells were monitored for changes in body weight for 32 days (h) The The same groups of mice were monitored for changes in blood glucose over the course of the experiment as indicated. Longitudinal body weight and glucose measurements in panels (b), (c), and (g) were analyzed by two-way repeated-measures ANOVA with Geisser–Greenhouse correction, with no significant differences observed between treatment groups. Glucose measurements in panel (h) were analyzed using a two-way mixed-effects model to accommodate missing observations; a modest group x time interaction was observed (p=0.040), with JEDI-treated mice exhibiting slightly lower glucose levels compared with controls. ANOVA, analysis of variance; EGFP, enhanced GFP; IHC, immunohistochemistry; JEDI, Just EGFP death-inducing.

due to T cell-directed killing of ARF-expressing cells in healthy tissues. Injection of JEDI T cells was well-tolerated regardless of ARF-GFP status, with similar maintenance of normal body weights recorded for JEDI or B10.D2 T cell-treated mice (figure 5b). As ARF can be expressed in some pancreatic beta cells,[55] blood glucose levels were also monitored, and no signs of glucose intolerance were observed for any group (figure 5c). To further evaluate the relative health of B10.D2 vs JEDI T cell treated mice, blood was collected on days 12 and 43 for a complete blood cell count (CBC) analysis (online supplemental figure 7a), and on day 36 serum was collected for a comprehensive metabolic panel (online supplemental figure 7b). No significant differences in blood cell lineages or metabolic markers were observed between treatment groups.

We then repeated this study using an alternative experimental design in which naïve JEDI T cells were injected into ARF-GFP mice and primed in vivo by vaccination with a lentivirus expressing GFP under a strong mouse stem cell virus (MSCV) promoter. Using this approach, previous studies have shown effective elimination of microglia in CX3CR1-EGFP mice, rare GFP-expressing cells in the heart of HCN4-GFP mice, and pancreatic beta cells in insulin promoter-GFP mice.[17] ARF-GFP$^+$ mice were injected IV with 10^8IU EGFP-expressing lentivirus and 5×10^6 naïve CD8$^+$ T cells from JEDI or B10.D2 mice (figure 5d). Analysis of spleens by immunohistochemistry (IHC) after 32 days revealed an extensive GFP signal in the spleens of mice that received GFP-expressing lentivirus and B10.D2 T cells (mean of 8.83% of all splenocytes expressed GFP across samples), but few GFP$^+$ cells in the spleens of mice that received JEDI T cells (mean of 1.92%) (figure 5e, online supplemental figure 8). Thus, the GFP-lentivirus induced efficient expression of GFP in the spleens of treated/vaccinated mice, resulting in JEDI T cell activation and subsequent lysis of GFP$^+$ splenocytes in vivo. JEDI but not B10.D2 T cells express the CD45.1 allele, allowing for quantification of transferred JEDI T cells in the blood of treated animals (figure 5f). Injected JEDI T cells expanded in response to vaccination, constituting 10%–20% of total CD8 T cells by day 7 and then contracting by day 31 (figure 5f). Again, we observed no difference in body weight between mice receiving JEDI or B10.D2 T cells (figure 5g), and glucose levels were not elevated in JEDI-treated mice, but instead were modestly lower over time compared with controls (figure 5h). Collectively, these data suggest that elimination of ARF-expressing cells by JEDI T cells in ARF-GFP mice is well tolerated, similar to previous models in which ARF or p16-expressing cells were eliminated in adult animals.[43 45–50] It may also be the case that very low expression of ARF in healthy adult tissues is insufficient to mediate lysis by JEDI T cells, which would also be consistent with a limited risk of on-target, off-tumor toxicity by ARF-specific TCR-T cells in vivo.

It remains possible that under abnormal conditions, stress-induced ARF expression in normal tissues could result in on-target off-tumor toxicity. Many cell types can activate the CDKN2A locus when cultured in vitro in response to replicative and stress-associated signals.[20] In vitro culture of renal cortical epithelial cells is known to promote both p16 and ARF protein expression,[21 56] and ARF protein expression by cultured airway epithelial cells has also been reported.[20] To characterize ARF3-6 TCR-T cell recognition of induced ARF expression in healthy tissue cell types, HLA-A2$^+$ bronchial epithelial and renal cortical epithelial cells, as well as induced pluripotent stem cell-derived astrocytes, were cultured in vitro for 3 weeks followed by coculture with ARF3-6 TCR-T cells in an Incucyte killing assay (online supplemental figure 9). No TCR-specific killing of in vitro cultured astrocytes or bronchial epithelial cells was observed. However, some TCR-T cell-mediated killing of cultured renal cortical epithelial cells was observed, likely reflecting lysis of ARF-expressing senescent cells.[57]

The ARF$_{35\text{-}43}$ peptide/HLA-A2 complex can be readily detected on the surface of patient-derived tumor samples

ARF is frequently expressed by many tumor types,[13] including almost all cases of HPV$^+$ cervical cancers.[11] To directly assess ARF protein expression levels in cervical cancer, 158 cervical tumor samples and 27 normal cervical tissue controls were stained with an ARF-specific antibody for IHC (figure 6a). Approximately 70% of tumor samples had readily detectable ARF protein, while all normal cervical tissue samples were negative for ARF protein expression (figure 6b). ARF was broadly expressed by positive tumors, with the majority (52%) expressing ARF in 100% of tumor cells (figure 6c), further highlighting the value of this protein as a therapeutic target. Targeting of ARF-expressing tumors with the ARF$_{35\text{-}43}$-specific TCR-T cells depends on presentation of that peptide by HLA-A2 on those tumors. To approximate the number of ARF$_{35\text{-}43}$ peptide/HLA-A2 complexes per cell that are associated with patient-derived tumor samples, primary cervical cancer samples from 20 HLA-A2 individuals were obtained, and specific HLA-associated peptides were quantitated by LC-MS as previously described.[58 59] The ARF$_{3543}$ peptide was readily detected in 16 of 20 samples (80%) (figure 6d), with 6 samples estimated to present 10–100 ARF$_{35\text{-}43}$ peptide/MHC complexes per cell, which is in line with other successfully targeted tumor-associated antigens.[28] One sample was predicted to present several hundred complexes per cell. Importantly, the ARF$_{35\text{-}43}$ peptide was not detected in a dataset of HLA-associated peptides from a panel of more than 40 normal tissues from 12 HLA-A2$^+$ donors (online supplemental table 3), confirming the lack of ARF presentation by normal tissues.

DISCUSSION

Tumor suppressor proteins safeguard cells from malignant transformation by triggering cell cycle arrest and apoptosis in response to abnormal growth signals and are therefore often disrupted in cancers through gene

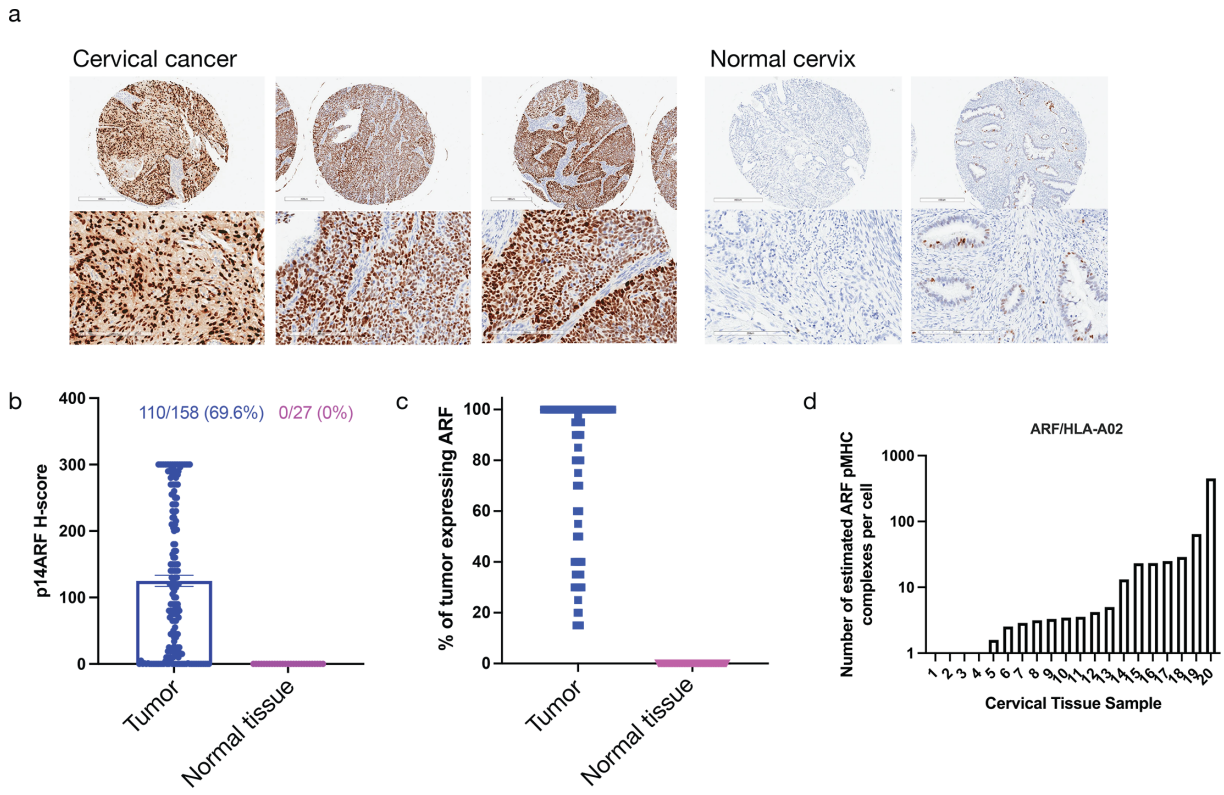

Figure 6 Detection of the ARF_{35-43} peptide/HLA-A2 complex in patient-derived tumor samples. 158 cervical tumor samples and 27 normal cervical tissue samples from a tissue microarray were stained with an ARF specific antibody. (a) ARF antibody staining of representative cervical cancer (left) and normal cervix samples. (b) ARF staining in each cervical tumor or normal tissue sample was calculated as an H-score, calculated as the sum of the intensity grade of staining (0–3) multiplied by the percentage of positive cells corresponding to each grade (1 × (% cells 1+) + 2 × (% cells 2+) + 3×(% cells 3+). This method gives a final H-score for ARF ranging from 0 to 300. (c) The percentage of cells staining positive for ARF within each ARF+sample (samples for which >10% of cells stained positive for ARF). Each dot represents a tumor/tissue sample with the corresponding percent ARF positivity indicated on the y-axis. 52% of cells were scored as 100% positive. (d) Primary cervical cancer samples from 20 HLA-A2 individuals were obtained, and the estimated number of HLA-associated ARF_{35-43} peptides per cell was quantitated by liquid chromatography–mass spectrometry (LC-MS).

deletion, mutation, or epigenetic silencing.[60] However, alterations in associated target genes or regulatory pathways can paradoxically drive overexpression of tumor suppressor proteins in some cancers. P21(CIP1/WAF1) is overexpressed in multiple tumors including a large fraction of esophageal squamous cell carcinomas,[61] many gliomas, and breast cancers[62], and tumors harboring inactivating mutations in p53 frequently show marked accumulation of p53 protein.[63] A previous study reported TCRs from mice targeting an unmutated human p53 epitope capable of broadly recognizing tumors with overexpressed p53,[64] and we have taken a similar approach, exploiting the overexpression of ARF in many tumors as a therapeutic target. Mechanistically, p16 and ARF are often overexpressed in cancers following inactivation of downstream targets Rb and p53, which normally enforce negative feedback regulation of p16 and ARF expression, respectively.[5 9 60 65]

ARF in particular is broadly expressed by many tumor types including a majority of all tumors with p53 mutations,[13] as active p53 normally represses oncogene-induced ARF expression.[5] ARF is expressed by most cervical cancers[11] and more than two-thirds of breast cancers.[12] Importantly, ARF expression is often homogenously expressed in these tumors. For example, a study evaluating samples from >1000 breast cancer patients by IHC reported high-level homogeneous expression of ARF in 77% of tumors, and we observed uniform expression of ARF protein in many primary cervical cancer samples (figure 6a and c). In contrast, ARF is not commonly expressed by normal adult tissues, with detectable expression restricted to mitotic spermatogonia in the testes and a small number of senescent cells in adults.[18 66] Furthermore, overexpression of ARF, but not p16, is associated with a worse prognosis in many human cancers and may contribute to the malignant phenotype.[8 67] Studies have shown that overexpressed ARF can enhance tumor development, supporting tumor growth and survival by inducing autophagy and activating pro-survival pathways[8]; and ARF can antagonize the tumor suppressing role of p16 by promoting p16 protein degradation.[68] Together, these findings suggest that therapeutic targeting of ARF could be remarkably effective and support the development of ARF-specific T cell-based therapeutics for many advanced cancers, especially HPV-associated cancers and the large number of cancers that have mutations in p53.

We have developed a high-affinity TCR-T cell-based therapeutic that targets the HLA-A2-restricted epitope ARF_{35-43} for the lysis of ARF-expressing tumor cells in vitro and in vivo. The ARF_{35-43} peptide was found to be broadly expressed in primary cervical cancer samples by LC-MS analysis, but not detected among HLA A2-associated peptides from normal tissues across multiple organs and donors, consistent with the limited expression of ARF in normal adult tissues.[18 66] While expression of ARF in non-transformed adult cells does occur in some senescent cell types,[69] multiple studies in genetically modified mice have established that elimination of p16- or ARF-expressing senescent cells in vivo is not detrimental. On the contrary, these studies reported beneficial outcomes including improved health and extended life span associated with the elimination of ARF or p16-expressing senescent cells.[43 45 47–49 70] ARF expression can also be induced in response to cellular stressors such as oncogenic stress, oxidative stress, or DNA damage. To model stress-induced ARF expression by non-transformed cells under abnormal conditions, cells from normal tissues were cultured for several weeks in vitro, which imposes multiple types of stress that can activate the CDKN2A locus. Neither cultured bronchial epithelial cells nor cultured astrocytes expressed sufficient ARF protein under these conditions to be recognized by ARF3-6 TCR-T cells. However, we did observe some TCR-T cell-mediated lysis of in vitro cultured renal cortical epithelial cells, which are known to express both p16 and ARF protein in response to in vitro culture. However, ARF is not normally expressed by these cells in vivo and is not induced during normal aging.[57] Rather, ARF expression in vivo is specifically associated with tubular atrophy, where accumulating ARF^{+} senescent cells drive inflammation and mediate tissue damage, causing a loss of renal function. Indeed, senolytic therapies designed to eliminate these senescent cells are currently under investigation as a treatment for diabetic kidney disease.[71]

To further explore the potential risks of eliminating ARF-expressing cells with adoptively transferred TCR-T cells, we developed a platform to study in vivo safety that takes advantage of the well-characterized JEDI mouse model.[17] $CD8^{+}$ T cells from JEDI mice have been shown to effectively eliminate cells expressing GFP under the control of various endogenous promoters in vivo, including efficient elimination of rare GFP^{+} cells with tissue-specific GFP expression.[17 51–53] Injecting JEDI T cells into mice that express GFP under ARF promoter control did not result in any detectable toxicity or damage to normal healthy tissues. Although this model requires heterozygous expression of the ARF promoter-driven GFP, which could lead to decreased GFP expression, we were able to detect GFP in both adult testes and senescent fibroblasts from ARF-GFP heterozygous mice, consistent with published studies.[41 42] These results further support the safety of therapeutically targeting ARF-expressing tumors with ARF-specific TCR-T cells.

In summary, the results of this study support the strategy of therapeutically targeting selected tumor suppressor proteins that become overexpressed when they can no longer suppress tumor cell growth and identify ARF_{35-43} as a promising tumor-specific HLA-A2-restricted T cell epitope that is broadly expressed and presented by many tumors. Eliminating tumor cells expressing ARF with adoptively transferred TCR-T cells is a promising strategy that could be broadly effective against a large number of tumor types, including some of the most aggressive and difficult to treat cancers.

Author affiliations
[1]Program in Immunology and Translational Science and Therapeutics Division, Fred Hutchinson Cancer Center, Seattle, Washington, USA
[2]Cullinan Therapeutics Inc, Cambridge, Massachusetts, USA
[3]Department of Immunology, University of Washington, Seattle, Washington, USA
[4]Translational Sciences and Therapeutics, Fred Hutch Cancer Center, Seattle, Washington, USA
[5]Department of Medicine, University of Washington, Seattle, Washington, USA

Acknowledgements We thank all members of the Chapuis and Greenberg lab for their contribution to the manuscript; the Fred Hutch Flow Cytometry and Cellular Imaging Comparative Medicine Shared Resources for their respective roles in helping to run key experiments. We would also like to thank Curtis McMurtrey from PureMHC for providing technical assistance and feedback on the manuscript.

Contributors Conception and design were performed by TMS, AGC, PAB, and JSM. TMS is the guarantor of the work. Experiments were designed and performed by TMS, KF, CB, AV, JS, MH, DHP, LT, JL, and BL. Data analysis and interpretation were performed by TMS, BL, JS, DHP, NKM, KR, KS, KAW, PAB, AGC, and PDG. TMS wrote the manuscript with input from all authors.

Funding This work was supported by funding from Cullinan Therapeutics (Fred Hutch Reference Number: SRA191002). KR, KAW, KS, and JSM are employed by Cullinan Therapeutics and contributed to study design, analysis and collection of data, and preparation of the manuscript. Cullinan Therapeutics did not influence the results/outcomes of the study despite author affiliations with the funder. PDG is supported by the Parker Institute for Cancer Immunotherapy, AGC is supported by the John C. and Karyl Kay Hughes Endowed Chair.

Competing interests TMS has received research support from Cullinan Therapeutics, which contributed to the design and preparation of this manuscript and has equity in Affini-T therapeutics. AGC has equity in Metagenomi and Affini-T Therapeutics. TMS and AGC have intellectual property related to the TCRs reported in this manuscript. PDG consults for and has equity interest in Affini-T Therapeutics, Rapt Therapeutics, Elpisciences, Immunoscape, Earli, Metagenomi. Catalia and Nextech. PAB consults for and has ownership interest in Cullinan Therapeutics. KR, KAW, KS, and JSM are employed by Cullinan Therapeutics. KR, KAW, KS, NKM and JSM own Cullinan stock. All other authors declare that they have no competing interests.

Patient consent for publication Not applicable.

Ethics approval All animal research in this study was approved under the Fred Hutchinson Cancer Center Institutional Animal Care and Use Committee protocol (IR# 50898).

Provenance and peer review Not commissioned; externally peer reviewed.

Data availability statement Data are available on reasonable request.

ORCID iDs
Thomas M Schmitt https://orcid.org/0000-0002-0736-4195
Kerry A Whalen https://orcid.org/0000-0001-8003-0346
Aude G Chapuis https://orcid.org/0000-0002-9574-5448

REFERENCES

1 Stromnes IM, Schmitt TM, Chapuis AG, *et al*. Re-adapting T cells for cancer therapy: from mouse models to clinical trials. *Immunol Rev* 2014;257:145–64.
2 Wang QJ, Yu Z, Griffith K, *et al*. Identification of T-cell Receptors Targeting KRAS-Mutated Human Tumors. *Cancer Immunol Res* 2016;4:204–14.
3 Vogelstein B, Papadopoulos N, Velculescu VE, *et al*. Cancer Genome Landscapes. *Science* 2013;339:1546–58.
4 Inoue K, A. Fry E. Aberrant expression of p16INK4a in human cancers – a new biomarker? *Cancer Rep Rev* 2018;2.
5 Stott FJ, Bates S, James MC, *et al*. The alternative product from the human CDKN2A locus, p14(ARF), participates in a regulatory feedback loop with p53 and MDM2. *EMBO J* 1998;17:5001–14.
6 Larsson LG. Oncogene- and tumor suppressor gene-mediated suppression of cellular senescence. *Semin Cancer Biol* 2011;21:367–76.
7 De Wispelaere N, Rico SD, Bauer M, *et al*. High prevalence of p16 staining in malignant tumors. *PLoS One* 2022;17:e0262877.
8 Fontana R, Ranieri M, La Mantia G, *et al*. Dual Role of the Alternative Reading Frame ARF Protein in Cancer. *Biomolecules* 2019;9:87.
9 Humbey O, Pimkina J, Zilfou JT, *et al*. The ARF tumor suppressor can promote the progression of some tumors. *Cancer Res* 2008;68:9608–13.
10 Li Y, Nichols MA, Shay JW, *et al*. Transcriptional repression of the D-type cyclin-dependent kinase inhibitor p16 by the retinoblastoma susceptibility gene product pRb. *Cancer Res* 1994;54:6078–82.
11 Kanao H, Enomoto T, Ueda Y, *et al*. Correlation between p14(ARF)/p16(INK4A) expression and HPV infection in uterine cervical cancer. *Cancer Lett* 2004;213:31–7.
12 Pare R, Shin JS, Lee CS. Increased expression of senescence markers p14(ARF) and p16(INK4a) in breast cancer is associated with an increased risk of disease recurrence and poor survival outcome. *Histopathology* 2016;69:479–91.
13 Kamijo T, Weber JD, Zambetti G, *et al*. Functional and physical interactions of the ARF tumor suppressor with p53 and Mdm2. *Proc Natl Acad Sci U S A* 1998;95:8292–7.
14 Zhang C, Liu J, Xu D, *et al*. Gain-of-function mutant p53 in cancer progression and therapy. *J Mol Cell Biol* 2020;12:674–87.
15 Kotsinas A, Papanagnou P, Evangelou K, *et al*. ARF: a versatile DNA damage response ally at the crossroads of development and tumorigenesis. *Front Genet* 2014;5:236.
16 Muss HB, Smitherman A, Wood WA, *et al*. p16 a biomarker of aging and tolerance for cancer therapy. *Transl Cancer Res* 2020;9:5732–42.
17 Agudo J, Ruzo A, Park ES, *et al*. GFP-specific CD8 T cells enable targeted cell depletion and visualization of T-cell interactions. *Nat Biotechnol* 2015;33:1287–92.
18 Lagopati N, Belogiannis K, Angelopoulou A, *et al*. Non-Canonical Functions of the ARF Tumor Suppressor in Development and Tumorigenesis. *Biomolecules* 2021;11:86.
19 Robins HS, Campregher PV, Srivastava SK, *et al*. Comprehensive assessment of T-cell receptor β-chain diversity in αβ T cells. *Blood* 2009;114:4099–107.
20 Smith JL, Lee LC, Read A, *et al*. One-step immortalization of primary human airway epithelial cells capable of oncogenic transformation. *Cell Biosci* 2016;6:57.
21 Berkenkamp B, Susnik N, Baisantry A, *et al*. In Vivo and In Vitro Analysis of Age-Associated Changes and Somatic Cellular Senescence in Renal Epithelial Cells. *PLoS ONE* 2014;9:e88071.
22 Reynisson B, Alvarez B, Paul S, *et al*. NetMHCpan-4.1 and NetMHCIIpan-4.0: improved predictions of MHC antigen presentation by concurrent motif deconvolution and integration of MS MHC eluted ligand data. *Nucleic Acids Res* 2020;48:W449–54.
23 Reuschenbach M, Pauligk C, Karbach J, *et al*. A phase 1/2a study to test the safety and immunogenicity of a p16(INK4a) peptide vaccine in patients with advanced human papillomavirus-associated cancers. *Cancer* 2016;122:1425–33.
24 Ho WY, Nguyen HN, Wolfl M, *et al*. In vitro methods for generating CD8+ T-cell clones for immunotherapy from the naïve repertoire. *J Immunol Methods* 2006;310:40–52.
25 Riddell SR, Watanabe KS, Goodrich JM, *et al*. Restoration of Viral Immunity in Immunodeficient Humans by the Adoptive Transfer of T Cell Clones. *Science* 1992;257:238–41.
26 Clutton GT, Weideman AMK, Mischell MA, *et al*. CD3 downregulation identifies high-avidity human CD8 T cells. *Clin Exp Immunol* 2024;215:279–90.
27 Liu Y, Johnson SM, Fedoriw Y, *et al*. Expression of p16INK4a prevents cancer and promotes aging in lymphocytes. *Blood* 2011;117:3257–67.
28 Bossi G, Gerry AB, Paston SJ, *et al*. Examining the presentation of tumor-associated antigens on peptide-pulsed T2 cells. *Oncoimmunology* 2013;2:e26840.
29 Almontashiri NAM, Fan M, Cheng BLM, *et al*. Interferon-γ Activates Expression of p15 and p16 Regardless of 9p21.3 Coronary Artery Disease Risk Genotype. *J Am Coll Cardiol* 2013;61:143–7.
30 Bassani-Sternberg M, Chong C, Guillaume P, *et al*. Deciphering HLA-I motifs across HLA peptidomes improves neo-antigen predictions and identifies allostery regulating HLA specificity. *PLoS Comput Biol* 2017;13:e1005725.
31 Hassan C, Kester MGD, de Ru AH, *et al*. The Human Leukocyte Antigen–presented Ligandome of B Lymphocytes. *Molecular & Cellular Proteomics* 2013;12:1829–43.
32 Shraibman B, Barnea E, Kadosh DM, *et al*. Identification of Tumor Antigens Among the HLA Peptidomes of Glioblastoma Tumors and Plasma. *Molecular & Cellular Proteomics* 2019;18:1255–68.
33 Moran AE, Holzapfel KL, Xing Y, *et al*. T cell receptor signal strength in Treg and iNKT cell development demonstrated by a novel fluorescent reporter mouse. *J Exp Med* 2011;208:1279–89.
34 Evans M, Borysiewicz LK, Evans AS, *et al*. Antigen Processing Defects in Cervical Carcinomas Limit the Presentation of a CTL Epitope from Human Papillomavirus 16 E6. *J Immunol* 2001;167:5420–8.
35 Berggren P, Kumar R, Sakano S, *et al*. Detecting homozygous deletions in the CDKN2A(p16(INK4a))/ARF(p14(ARF)) gene in urinary bladder cancer using real-time quantitative PCR. *Clin Cancer Res* 2003;9:235–42.
36 Border EC, Sanderson JP, Weissensteiner T, *et al*. Affinity-enhanced T-cell receptors for adoptive T-cell therapy targeting MAGE-A10: strategy for selection of an optimal candidate. *Oncoimmunology* 2019;8:e1532759.
37 Karlsson M, Zhang C, Méar L, *et al*. A single-cell type transcriptomics map of human tissues. *Sci Adv* 2021;7:eabh2169.
38 Tsherniak A, Vazquez F, Montgomery PG, *et al*. Defining a Cancer Dependency Map. *Cell* 2017;170:564–76.
39 Lahman MC, Schmitt TM, Paulson KG, *et al*. Targeting an alternate Wilms' tumor antigen 1 peptide bypasses immunoproteasome dependency. *Sci Transl Med* 2022;14:eabg8070.
40 McKeller RN, Fowler JL, Cunningham JJ, *et al*. The Arf tumor suppressor gene promotes hyaloid vascular regression during mouse eye development. *Proc Natl Acad Sci U S A* 2002;99:3848–53.
41 Zindy F, Quelle DE, Roussel MF, *et al*. Expression of the p16INK4a tumor suppressor versus other INK4 family members during mouse development and aging. *Oncogene* 1997;15:203–11.
42 Zindy F, Williams RT, Baudino TA, *et al*. Arf tumor suppressor promoter monitors latent oncogenic signals in vivo. *Proc Natl Acad Sci U S A* 2003;100:15930–5.
43 Mikawa R, Suzuki Y, Baskoro H, *et al*. Elimination of $p19^{ARF}$-expressing cells protects against pulmonary emphysema in mice. *Aging Cell* 2018;17:e12827.
44 Varghese SS, Dhawan S. Senescence: a double-edged sword in beta-cell health and failure? *Front Endocrinol (Lausanne)* 2023;14:1196460.
45 Hashimoto M, Asai A, Kawagishi H, *et al*. Elimination of $p19^{ARF}$-expressing cells enhances pulmonary function in mice. *JCI Insight* 2016;1:e87732.
46 Aguayo-Mazzucato C, Andle J, Lee TB Jr, *et al*. Acceleration of β Cell Aging Determines Diabetes and Senolysis Improves Disease Outcomes. *Cell Metab* 2019;30:129–42.
47 Baker DJ, Wijshake T, Tchkonia T, *et al*. Clearance of p16Ink4a-positive senescent cells delays ageing-associated disorders. *Nature New Biol* 2011;479:232–6.
48 Bussian TJ, Aziz A, Meyer CF, *et al*. Clearance of senescent glial cells prevents tau-dependent pathology and cognitive decline. *Nature New Biol* 2018;562:578–82.
49 Guzman SD, Judge J, Shigdar SM, *et al*. Removal of p16INK4 Expressing Cells in Late Life has Moderate Beneficial Effects on Skeletal Muscle Function in Male Mice. *Front Aging* 2021;2:821904.
50 Lewis-McDougall FC, Ruchaya PJ, Domenjo-Vila E, *et al*. Aged-senescent cells contribute to impaired heart regeneration. *Aging Cell* 2019;18:e12931.

51 Borroni E, Borsotti C, Cirsmaru RA, *et al*. Immune tolerance promotion by LSEC-specific lentiviral vector-mediated expression of the transgene regulated by the stabilin-2 promoter. *Mol Ther Nucleic Acids* 2024;35:102116.
52 Chen A, Lee K, D'Agati VD, *et al*. Bowman's capsule provides a protective niche for podocytes from cytotoxic CD8+ T cells. *J Clin Invest* 2018;128:3413–24.
53 Strine MS, Fagerberg E, Darcy PW, *et al*. Intestinal tuft cell immune privilege enables norovirus persistence. *Sci Immunol* 2024;9:eadi7038.
54 Zindy F, Eischen CM, Randle DH, *et al*. Myc signaling via the ARF tumor suppressor regulates p53-dependent apoptosis and immortalization. *Genes Dev* 1998;12:2424–33.
55 Chen H, Gu X, Su I, *et al*. Polycomb protein Ezh2 regulates pancreatic beta-cell Ink4a/Arf expression and regeneration in diabetes mellitus. *Genes Dev* 2009;23:975–85.
56 Zhou S, Ling X, Meng P, *et al*. Cannabinoid receptor 2 plays a central role in renal tubular mitochondrial dysfunction and kidney ageing. *J Cellular Molecular Medi* 2021;25:8957–72.
57 Melk A, Schmidt BMW, Takeuchi O, *et al*. Expression of p16INK4a and other cell cycle regulator and senescence associated genes in aging human kidney. *Kidney Int* 2004;65:510–20.
58 Hoover AR, Kaabinejadian S, Krawic JR, *et al*. Localized ablative immunotherapy drives de novo $CD8^+$ T-cell responses to poorly immunogenic tumors. *J Immunother Cancer* 2022;10:e004973.
59 Purcell AW, Ramarathinam SH, Ternette N. Mass spectrometry-based identification of MHC-bound peptides for immunopeptidomics. *Nat Protoc* 2019;14:1687–707.
60 Liggett WH, Sidransky D. Role of the p16 tumor suppressor gene in cancer. *J Clin Oncol* 1998;16:1197–206.
61 Goan YG, Hsu HK, Chang HC, *et al*. Deregulated p21(WAF1) overexpression impacts survival of surgically resected esophageal squamous cell carcinoma patients. *Ann Thorac Surg* 2005;80:1007–16.
62 Abbas T, Dutta A. p21 in cancer: intricate networks and multiple activities. *Nat Rev Cancer* 2009;9:400–14.
63 Vousden KH, Lane DP. p53 in health and disease. *Nat Rev Mol Cell Biol* 2007;8:275–83.
64 Liu X, Peralta EA, Ellenhorn JD, *et al*. Targeting of human p53-overexpressing tumor cells by an HLA A*0201-restricted murine T-cell receptor expressed in Jurkat T cells. *Cancer Res* 2000;60:693–701.
65 Evangelou K, Bartkova J, Kotsinas A, *et al*. The DNA damage checkpoint precedes activation of ARF in response to escalating oncogenic stress during tumorigenesis. *Cell Death Differ* 2013;20:1485–97.
66 Carrasco-Garcia E, Moreno M, Moreno-Cugnon L, *et al*. Increased Arf/p53 activity in stem cells, aging and cancer. *Aging Cell* 2017;16:219–25.
67 Dong Y, Zheng M, Wang X, *et al*. High expression of CDKN2A is associated with poor prognosis in colorectal cancer and may guide PD-1-mediated immunotherapy. *BMC Cancer* 2023;23:1097.
68 Kobayashi T, Wang J, Al-Ahmadie H, *et al*. ARF Regulates the Stability of p16 Protein Via REGγ-Dependent Proteasome Degradation. *Mol Cancer Res* 2013;11:828–33.
69 Carlos AR, Escandell JM, Kotsantis P, *et al*. ARF triggers senescence in Brca2-deficient cells by altering the spectrum of p53 transcriptional targets. *Nat Commun* 2013;4:2697.
70 Patil P, Dong Q, Wang D, *et al*. Systemic clearance of $p16^{INK4a}$ -positive senescent cells mitigates age-associated intervertebral disc degeneration. *Aging Cell* 2019;18:e12927.
71 Palmer AK, Tchkonia T, Kirkland JL. Senolytics: Potential for Alleviating Diabetes and Its Complications. *Endocrinology* 2021;162:bqab058.